Determining the style and provenance of magmatic activity during the Early Aptian Oceanic Anoxic Event (OAE 1a)

Percival, Lawrence; Tedeschi, Leonardo; Creaser, Robert; Bottini, Cinzia; Erba, Elisabetta; Giraud, Fabienne; Svensen, Henrik; Savian, Jairo; Trindade, Ricardo; Coccioni, Rodolfo; Frontalini, Fabrizio; Jovane, Luigi; Mather, Tamsin; Jenkyns, Hugh

Published in:
Global and Planetary Change

DOI:
10.1016/j.gloplacha.2021.103461

Publication date:
2021

Determining the style and provenance of magmatic activity during the Early Aptian Oceanic Anoxic Event (OAE 1a)

L.M.E. Percival[1]*; L.R. Tedeschi[2]; R.A. Creaser[3]; C. Bottini[4]; E. Erba[4]; F. Giraud[5]; H. Svensen[6]; J. Savian[7]; R. Trindade[8]; R. Coccioni[9]; F. Frontalini[10]; L. Jovane[11]; T.A. Mather[12]; H.C. Jenkyns[12]

1: Analytical, Environmental and Geochemistry (AMGC) Group, Vrije Universiteit Brussel, Pleinlaan 2, 1050 Brussels, Belgium

2: Centro de Pesquisas e Desenvolvimento Leopoldo Américo Miguez de Mello (CENPES), Petróleo Brasileiro S.A., Avenida Horácio Macedo 950, 21941-915 Rio de Janeiro, Brazil

3: Department of Earth and Atmospheric Sciences, University of Alberta, Edmonton, Alberta, T6G 2E3, Canada

4: Dipartimento di Scienze della Terra, Università degli Studi di Milano, 20133 Milan, Italy

5: Université Grenoble Alpes, IRD, Université Savoie Mont Blanc, CNRS, Université Gustave Eiffel, ISTerre, 38000 Grenoble, France

6: The Center for Earth Evolution and Dynamics, University of Oslo, PO Box 1028 Blindern, 0315 Oslo, Norway

7: Departamento de Geologica, Universidade Federal do Rio Grande do Sul, 91501-970 Porto Alegre, Brazil

8: Departamento de Geofísica, Universidade de São Paulo, 05508-090 São Paulo, Brazil

9: Università degli Studi di Urbino "Carlo Bo", 61029 Urbino, Italy

10: Dipartimento di Scienze Pure e Applicate, Università degli Studi di Urbino "Carlo Bo", 61029 Urbino, Italy

11: Instituto Oceanográfico, Universidade de São Paulo, 05508-120 São Paulo, Brazil

12: Department of Earth Sciences, University of Oxford, South Parks Road, Oxford, OX1 3AN, UK

*Corresponding author: lawrence.percival@vub.be

KEYWORDS

Early Aptian Oceanic Anoxic Event (OAE 1a); mercury; osmium isotopes; Greater Ontong-Java Plateau; High Arctic Large Igneous Province; submarine LIP volcanism

ABSTRACT

Large igneous province (LIP) volcanism has been proposed as a key trigger of several major climate and environmental perturbations during the Phanerozoic Aeon. Large-scale carbon emissions associated with one or both of magmatic degassing from the Greater Ontong-Java Plateau (G-OJP) and intrusion of organic-rich sediments by High Arctic LIP (HALIP) sills have been widely suggested as the trigger of the Early Aptian Oceanic Anoxic Event (OAE 1a: ~120 Ma). However, the respective roles of the two LIPs and associated carbon sources in causing this crisis remain debated. Here, six records of OAE 1a from the Pacific, Tethyan, Arctic, and South Atlantic realms are investigated, combining mercury (Hg) concentrations and osmium-(Os-) isotope ratios as proxies of LIP activity. Together with previously published datasets, the results indicate globally consistent Os-isotope evidence for LIP activity during OAE 1a, but geographically variable stratigraphic Hg trends. Clear mercury enrichments that match Os-isotope evidence of LIP activity, and suggest a Hg-cycle perturbation during the onset of OAE 1a, are documented at one Pacific site extremely proximal to the G-OJP, but not in Arctic, Tethyan or Atlantic records. This pattern highlights significant G-OJP volcanism during the onset of OAE 1a, and re-emphasises the limited potential for submarine LIP eruptions to cause Hg-cycle perturbations except in areas very proximal to source. The absence of clear Hg peaks in basal OAE 1a strata from the Arctic (or anywhere outside of the Pacific) does not support intense HALIP activity at that time, suggesting that the G-OJP was the more volcanically active LIP when OAE 1a commenced. Thus, G-OJP emissions of mantle carbon were more likely to have played a major role in initiating OAE 1a than thermogenic volatiles associated with the HALIP. A transient pulse of HALIP-related subaerial eruptions and/or thermogenic volatile emissions during the early–middle part of OAE 1a, potentially evidenced by more widespread Hg enrichments in strata from that time (including in the Arctic), might have prolonged the event. However, a non-volcanic cause of these later Hg influxes cannot be excluded. These findings

challenge previous suggestions that magmatic CO_2 emissions from LIPs were incapable of causing major carbon-cycle perturbations alone, and highlight the need for further investigations to establish whether the high volume/emplacement rate of the G-OJP (potentially an order of magnitude greater than other LIPs) made it a unique case that stands in contrast to other provinces where the role of thermogenic volatiles was likely more crucial.

1. INTRODUCTION

Episodes of abrupt environmental perturbation occurred frequently throughout the Mesozoic Era, punctuating and/or superimposed upon longer term changes in climate (e.g., Jenkyns, 2010). The Early Aptian Oceanic Anoxic Event (OAE 1a, ~120 Ma) represented one of the most severe of these crises. Lasting ~1–1.4 Myr (Li *et al*., 2008; Malinverno *et al*., 2010), the event was characterized by the development of oxygen-depleted water columns across large parts of the global ocean and epicontinental shelf seas (e.g., Schlanger and Jenkyns, 1976; Weissert, 1989; Jenkyns, 1995; Pancost *et al*., 2004; Föllmi *et al*., 2006; van Breugel *et al*., 2007). Ocean acidification, global temperature changes, accelerated hydrological cycling, and enhanced continental weathering rates have also been proposed to have occurred at that time (e.g., Erba, 2004; Ando *et al*., 2008; Erba *et al*., 2010, 2015; Bottini *et al*., 2012, 2015; Hönisch *et al*., 2012; Mutterlose *et al*., 2014; Lechler *et al*., 2015; Naafs and Pancost, 2016; Jenkyns, 2018). The various environmental perturbations are thought to have arisen from (and in some cases, contributed to) severe carbon-cycle disturbances. These perturbations are reflected by a series of carbon-isotope ($\delta^{13}C$) excursions documented from lower Aptian strata that record OAE 1a; typically interpreted via comparison to segments (C1–C7) in the stratigraphic $\delta^{13}C$ trends first recorded in Tethyan pelagic sedimentary archives (Menegatti *et al*., 1998; see also Figure 1A, and Weissert, 1989; Jenkyns, 1995; Gröcke *et al*., 1999; Ando *et al*., 2008; Robinson *et al*., 2008; Vickers *et al*., 2016). Relatively stable $\delta^{13}C$ values spanning uppermost Barremian–lowermost Aptian strata (C1–C2) give way to a pronounced negative excursion in basal OAE 1a strata (C3), which is followed

by two distinct positive excursions (C4 and C6) that are locally separated by strata featuring stable carbon-isotope ratios higher than those of C2 (C5), and are succeeded by a continuation of high $\delta^{13}C$ values (C7) above the OAE 1a stratigraphic level (Menegatti *et al*., 1998; see also Figure 1A).

The two positive $\delta^{13}C$ excursions that typically signify the C4 and C6 segments are thought to record enhanced rates of organic-matter burial in the widespread anoxic–euxinic water columns that characterized OAE 1a (e.g., Weissert, 1989; Menegatti *et al*., 1998). Such organic-matter deposition is further evidenced by the preservation of organic-rich shales in several stratigraphic archives of the event worldwide (e.g., Schlanger and Jenkyns, 1976; Erba and Larson, 1998; Dumitrescu and Brassell, 2006; Hu *et al*., 2012; Robinson *et al*., 2017). Initially recognized in the Umbria–Marche Basin of Italy (Coccioni *et al*., 1987), the organic-rich shale unit is named the Selli Level in that region, with sedimentary rocks of OAE 1a age (whether comprising organic-rich shales or otherwise) elsewhere around the world dubbed the Selli Level Equivalent (see Figure 1 and Study Areas section).

By contrast, the C3 negative $\delta^{13}C$ shift is attributed to a pronounced flux of isotopically light carbon to the ocean–atmosphere system that likely initiated the environmental perturbations associated with OAE 1a (e.g., Jahren *et al*., 2001; Méhay *et al*., 2009; Kuhnt *et al*., 2011; Naafs *et al*., 2016). The source of this isotopically light carbon remains debated. Several authors have linked the carbon emissions to the emplacement of one or more large igneous provinces (LIPs) during earliest Aptian times, particularly the Greater Ontong-Java Plateau (G-OJP; Figure 2; see e.g., Erba, 1994; Larson and Erba, 1999; Tejada *et al*., 2009; Kuroda *et al*., 2011; Bottini *et al*., 2012; Erba *et al*., 2015; Polteau *et al*., 2016).

Geochemical modelling by Bauer *et al.* (2017) indicated that the emplacement of the G-OJP resulted in a geologically rapid six- to ten-fold increase in submarine volcanic activity during OAE 1a, and that such volcanism could have caused a fourfold rise in mantle carbon emissions ($\delta^{13}C \sim -6$ ‰; Gales *et al*., 2020, and references therein). These emissions alone could have plausibly caused a similarly swift 3000 ppm increase in atmospheric pCO_2 levels and the 1.5–2 ‰ negative $\delta^{13}C$ excursion

typically documented in the C3 segment. However, based on pCO_2 trends reconstructed from the Cau section (Betic Cordillera, Spain), Naafs *et al*. (2016) argued that pCO_2 levels only rose gradually through the first part of OAE 1a and by <300 ppm during the C3 segment. In this case, a much smaller increase in carbon emissions, but with a very isotopically light composition ($\delta^{13}C < -10$ ‰), would have been required to cause the C3 negative excursion without greatly increasing atmospheric pCO_2 (Adloff *et al*., 2020). Such parameters are inconsistent with a purely mantle-carbon source. Instead, this carbon could have been emitted following metamorphism of organic-rich sediments by intrusive sills during the emplacement of the High Arctic large igneous province (HALIP; Figure 2), or from the destabilisation of methane clathrates (e.g., Jahren *et al*., 2001; Méhay *et al*., 2009; Polteau *et al*., 2016; Adloff *et al*., 2020). This study investigates the geochemical records of volcanism related to the emplacement of the G-OJP and HALIP during the earliest Aptian and OAE 1a in order to determine the dominant style of magmatic activity operating during those times. This distinction might indicate whether or not a specific igneous province was the foremost source of carbon to the ocean–atmosphere system and likely the key trigger of the event.

1.1 Large Igneous Provinces emplaced during the latest Barremian and early Aptian

The G-OJP was an oceanic LIP consisting of several million cubic kilometres of igneous material (largely tholeiitic basalt) emplaced as intrusive and extrusive magma bodies into/onto the ocean crust of the western Pacific (Figure 2; see also Larson, 1991; Larson and Erba, 1999). The Ontong-Java Plateau alone has an immense volume of 10s of millions of cubic kilometres (possibly up to $44–57\times10^6$ km^3; Gladczenko *et al*., 1997). When other subsidiary plateaus thought to have initially formed as part of the G-OJP are included (e.g., the Manihiki and Hikurangi; Taylor, 2006; Hoernle *et al*., 2010), the total volume of igneous material rises to $59–77\times10^6$ km^3 (Kerr and Mahoney, 2007). The original province may have been even larger if a part of it was emplaced into/onto the now-subducted Farallon Plate, as has been previously suggested (Schlanger *et al*., 1981; Larson, 1991). Thus, the G-OJP could have been an order of magnitude greater in size than the largest-known continental LIPs: the

Siberian Traps and Central Atlantic Magmatic Province, which were likely no more than ~5×10^6 km^3 each in volume (see review by Bond and Wignall, 2014). The average eruption rate on the G-OJP remains unknown. However, if Bauer *et al.*'s (2017) calculation of a six- to ten-fold increase in submarine volcanic activity during OAE 1a compared to pre-OAE background mid-ocean ridge volcanism is correct, and ridge basalt production during Barremian–Aptian times was similar to today (~20 km^3/yr; Cogné and Humler, 2006), then on average >100 km^3/yr of igneous material would have been emplaced on the G-OJP during OAE 1a. This average eruption rate is markedly higher than that proposed for any known continental LIP (e.g., Schoene *et al.*, 2019).

By contrast, Barremian–Aptian HALIP magmatism apparently consisted chiefly of subaerially erupted basalt flows and the intrusion of tholeiitic sills into organic-rich sedimentary rocks (Tegner *et al.*, 2011; Corfu *et al.*, 2013; Polteau *et al.*, 2016; Dockman *et al.*, 2018). The volume of HALIP igneous material emplaced during Barremian–Aptian times remains poorly constrained, but is thought to have been on the order of 100,000s of cubic kilometres (Tegner *et al.*, 2011; Polteau *et al.*, 2016; Dockman *et al.*, 2018), much smaller than the G-OJP but more comparable in volume to many other LIPs. However, the intrusion of organic-rich sediments by HALIP magmatic sills could have acted as an additional source of isotopically light carbon ($\delta^{13}C$ < -20 ‰) to the ocean–atmosphere system (Polteau *et al.*, 2016; c.f., Svensen *et al.*, 2004; McElwain *et al.*, 2005). By contrast, carbon emissions from the G-OJP would have been almost exclusively magmatic in origin, as that LIP was predominantly emplaced into comparatively volatile-depleted oceanic basalts.

Crucially, although there is some evidence from phreatomagmatic deposits dated to ~120 Ma for subaerial eruptions on the G-OJP during Barremian–Aptian times (Chambers *et al.*, 2004; Thordarson, 2004), the emplacement of that province into/onto the oceanic crust means that the great majority of volcanic activity associated with it is expected to have been submarine in nature. By contrast, most volatile emissions from HALIP subaerial basalts and thermogenic degassing should have reached the atmosphere. Previous studies have highlighted the fact that geochemical markers of LIP

volcanism in stratigraphic archives may be able to distinguish between these styles of magmatic processes, and also yield information on the proximity of the igneous activity (Kuroda *et al.*, 2011; Erba *et al.*, 2015). In particular, Percival *et al.* (2018) noted the differing degrees to which styles of volcanism can affect the likelihood of LIP emplacement and associated eruptions being recorded by two key proxies for these phenomena: mercury (Hg) concentrations and osmium- (Os-) isotope ratios (specifically $^{187}Os/^{188}Os$).

1.2 Sedimentary $^{187}Os/^{188}Os$ ratios as a marker of LIP emplacement during OAE 1a

Large igneous province emplacement can cause a change in the $^{187}Os/^{188}Os$ composition of the global ocean by acting as a major source of mantle-derived osmium, through either direct emission of the element during submarine volcanic/hydrothermal activity or weathering/alteration of juvenile LIP basalts (e.g., Cohen and Coe, 2002; Turgeon and Creaser, 2008). Importantly, the seawater residence time of osmium (on the order of 10s kyr today: Peucker-Ehrenbrink and Ravizza, 2000) means that the global ocean should feature a homogenous $^{187}Os/^{188}Os$ composition but still respond to geologically rapid changes in the sources to that inventory, except in hydrographically restricted basins with a very low basin–ocean water-mass exchange where the Os-isotope ratio might be dominated by local inputs (e.g., Paquay and Ravizza, 2012; Dickson *et al.*, 2015).

Primitive osmium derived from mantle or meteoritic material features $^{187}Os/^{188}Os$ ~0.13 (Allègre *et al.*, 1999), whereas riverine osmium sourced from weathering of the continental crust is typically much more radiogenic (modern-day average riverine $^{187}Os/^{188}Os$ ~1.4; Peucker-Ehrenbrink and Jahn, 2001). Consequently, a significant increase in the flux of mantle-derived Os from LIP activity to the global ocean, relative to riverine runoff of the element from weathering of the continental crust and the comparatively consistent mid-ocean-ridge and cosmogenic inputs, should result in a lower seawater $^{187}Os/^{188}Os$ ratio throughout the open ocean. This hydrogenous Os-isotope signature is

193 recorded in seafloor sediments, which can preserve past seawater compositions as long as the
194 sedimentary system remains closed with respect to rhenium and osmium following deposition (Cohen
195 *et al*., 1999).
196
197 In all previously studied records of OAE 1a, a pronounced shift is observed in the recorded
198 seawater Os-isotope ratio ($^{187}Os/^{188}Os_{(i)}$) towards very unradiogenic compositions (typically <0.2)
199 around the base of the Selli Level or equivalent strata deposited during OAE 1a, together with an
200 increase in sedimentary Os concentrations (Tejada *et al*., 2009; Bottini *et al*., 2012; Adloff *et al*., 2020;
201 see also Figure 1B). These unradiogenic $^{187}Os/^{188}Os_{(i)}$ compositions and high Os concentrations
202 generally continue up the stratigraphy through the entire Selli Level (or equivalent), and are thought to
203 document intense LIP volcanism that acted as a source of osmium to the global ocean through one or
204 both of submarine hydrothermal emissions of the element and erosion/alteration of the juvenile basalts
205 formed during the volcanic activity (Tejada *et al*., 2009; Bottini *et al*., 2012; Adloff *et al*., 2020).
206 However, Tethyan records of OAE 1a also document a brief rebound in Os-isotope ratios to higher
207 values in basal Selli Level (or equivalent) strata, potentially highlighting a transient spell of enhanced
208 continental weathering and associated flux of radiogenic Os at the onset of the event that temporarily
209 overprinted the unradiogenic signature (Tejada *et al*., 2009; Bottini *et al*., 2012). This transient pulse of
210 enhanced continental weathering early in OAE 1a is supported by strontium- and lithium-isotope
211 excursions (Jones and Jenkyns, 2001; Lechler *et al*., 2015).
212
213
214 *1.3 Sedimentary Hg concentrations as a marker of LIP volcanism during OAE 1a*
215
216 Volcanic eruptions represent one of the largest natural sources of mercury to the Earth's surface
217 in the present day (Pyle and Mather, 2003; Bagnato *et al*., 2007). Mercury is chiefly emitted as a gaseous
218 elemental species that typically has a residence time of 0.5–2 years in the stratosphere, enabling
219 worldwide distribution before the element is ultimately deposited in sediments (Schroeder and Munthe,
220 1998; Ericksen *et al*., 2003; Selin *et al*., 2009). The global distribution of volcanic mercury has led

several studies of geological events associated with LIPs to utilise sedimentary concentrations of the element as a proxy for the volcanism (see reviews by Grasby *et al*., 2019; Percival *et al*., 2021). This approach includes normalising sedimentary mercury concentrations against total organic carbon (TOC) content to account for the association of the element with organic compounds when it is deposited in sediments (Sanei *et al*., 2012, and references therein). Thus, peaks in sedimentary Hg/TOC ratios are generally interpreted as reflecting an increased input of Hg to the environment from an external source, such as volcanism or wildfires, the latter of which is also known to cause peaks in sedimentary Hg and Hg/TOC values in modern settings (e.g., Daga *et al*., 2016).

However, in euxinic settings where free sulphides precipitate in the water column, Hg may be deposited with that phase rather than organic matter (Shen *et al*., 2019a; Shen *et al*., 2020). Alternatively, in a very well-oxygenated environment, featuring limited burial of both phases, mercury might be adsorbed on to clays (Kongchum *et al*., 2011; Shen *et al*., 2020). Even in settings where Hg contents follow those of TOC, a change in the type of organic matter (e.g., from marine bacterial to terrestrial detrital), or a large influx of organic material from a new source, could alter the Hg/TOC ratio if the affinity of mercury for the various kinds of organic material varies (see Hammer *et al*., 2019; Them *et al*., 2019). Therefore, robustly demonstrating a global-scale perturbation to the mercury signature caused by volcanism is dependent on documenting enrichment of the element in stratigraphic archives that cover a wide range of geographic areas, and for which the depositional environment and burial history are known.

To date, three stratigraphic archives of OAE 1a have been investigated for mercury and Hg/TOC trends by Charbonnier and Föllmi (2017), all of them representing palaeoenvironments from the north-westernmost part of the Tethyan realm: La Bédoule (South Provençal Basin, SE France), Glaise (Vocontian Basin, SE France), and Roter Sattel (Briançonnais Domain, Switzerland). This last record has been shown as being rather thermally mature (Charbonnier *et al*., 2018a), potentially altering the TOC content and inflating measured Hg/TOC ratios to above those from the time of deposition (as shown for other Cretaceous records by Charbonnier *et al*., 2020). Nonetheless, Charbonnier and Föllmi

(2017) reported increased Hg and Hg/TOC values that were ascribed to G-OJP volcanic activity during OAE 1a (see also Supplementary Figure 1). Interestingly, Barremian–Aptian boundary records from the northwest Tethyan area have also been hypothesized as recording an earlier episode of volcanism associated with that LIP, which took place significantly prior to OAE 1a (Charbonnier *et al*., 2018b).

1.4 Study aims

Whilst mercury-cycle perturbations from Barremian–Aptian times (including OAE 1a) have been reported from the northwest Tethyan area, and linked to volcanism on the G-OJP, it remains unclear whether these disturbances truly represent a global volcanic signal or local influxes of mercury to that specific region. In this context, it is notable that mercury emitted from modern submarine volcanic systems appears to be efficiently scavenged, limiting dispersal of the element from such sources to areas relatively proximal to the point(s) of origin (within 100s km; Bowman *et al*., 2015). Indeed, prior investigations of the latest Cenomanian OAE (OAE 2; ~94 Ma), which has also been linked with submarine LIP volcanism during oceanic-plateau emplacement (e.g., Turgeon and Creaser, 2008), have shown that most studied records of that event do not feature Hg enrichments or elevated Hg/TOC ratios, except perhaps for sites proximal to LIPs (Scaife *et al*., 2017; Percival *et al*., 2018).

Consequently, analyses of stratigraphic archives of OAE 1a from around the world are needed in order to determine whether there was global-scale Hg-cycle perturbation during that event, or localized disturbances unrelated to magmatism. Furthermore, a global perspective of the mercury cycle will help to elucidate whether any volcanic fluxes of mercury were largely derived from G-OJP or HALIP activity. If volatile emissions during OAE 1a were primarily associated with submarine LIP activity of the G-OJP, sedimentary mercury enrichments correlative with the Os-isotope evidence of volcanism would likely be recorded in Pacific sites proximal to that source, but potentially nowhere else due to the limited dispersal range of the element in the marine realm. By contrast, mercury fluxes

from subaerial eruptions and/or thermogenic emissions related to the HALIP should certainly be documented in the Arctic, and might also be documented in sites around the world due to those magmatic processes being more likely to emit volatiles directly to the atmosphere.

Here, new mercury data are presented from six records of latest-Barremian–early Aptian age, including OAE 1a (Figure 2): DSDP Site 463 (Mid-Pacific Mountains), the Cismon core (Belluno Basin, Italy), the Poggio le Guaine core (Umbria–Marche Basin, Italy), the Notre-Dame-de-Rosans section (Vocontian Basin, SE France), the DH-1 Longyearbyen core (Boreal Basin, Svalbard), and the Petrobras Well D (Sergipe-Alagoas Basin, NE Brazil). New Os-isotope data are also presented from the Poggio le Guaine core. These sequences include the first OAE 1a records from outside the Tethyan region that have been studied for mercury, offering a more global perspective on any Hg-cycle perturbations during that time. Crucially, these study areas include three sites where stratigraphic Hg and Os-isotope trends can be directly correlated (DSDP Site 463 and the Cismon and Poggio le Guaine cores). Additionally, the Mid-Pacific Mountain and Arctic sites would have been relatively proximal to the G-OJP and HALIP, respectively. Comparing these new mercury and osmium-isotope profiles with previously published datasets, and correlating trends in the two proxies amongst records where both have been studied, will give new insights on the dominant style of volcanic activity that influenced the global Hg cycle during OAE 1a and could potentially identify the LIP that was the primary trigger of that event.

2 STUDY AREAS

2.1 DSDP Site 463 (Mid-Pacific Mountains, W Pacific Ocean)

DSDP Site 463, drilled in the Mid-Pacific Mountains in 1978, records a large part of the uppermost Barremian to lower Aptian stratigraphic interval (Thiede *et al*., 1981). The lithology

generally consists of pelagic limestones with some chert-rich intervals (Mélières *et al*., 1981). There is a switch to more clay-rich marlstones between ~625–615 mbsf that marks the OAE 1a stratigraphic interval (Thiede *et al*., 1981; Sliter, 1989). However, black shales akin to those observed in most Tethyan archives are largely absent from this site and only appear in upper Selli Level Equivalent strata, with a modest increase in TOC content (to 1.5 wt%, *this study*; although previous works have reported values locally up to 7–8 wt%; Thiede *et al*., 1981; van Breugel *et al*., 2007; Bottini *et al*., 2012). Age constraints (including the position of the Barremian–Aptian boundary) are based largely on magneto- and biostratigraphy (Tarduno *et al*., 1989). Several studies have investigated the Barremian–Aptian carbon-isotope trends at DSDP Site 463 (e.g., Price, 2003; Ando *et al*., 2008; Bottini *et al*., 2012), identifying the C2–C7 segments that can be used to define the Selli Level Equivalent strata deposited during OAE 1a. Osmium-isotope trends and trace-metal enrichments have been interpreted as evidence for intense volcanic activity during Barremian–Aptian times (particularly before and during OAE 1a), with the volcanism generally attributed to the nearby G-OJP (Bottini *et al*., 2012; Erba *et al*., 2015). Volcanic eruptions proximal to DSDP Site 463 are supported by sporadic preservation of thin tuffaceous layers locally preserved within the Barremian–Aptian sediments, particularly within the Selli Level Equivalent (Hein and Vanek, 1981; Vallier and Jefferson, 1981; Thiede *et al*., 1982). The provenance of these tuffs remains unknown, but given the proximity of the Mid-Pacific Mountains to the G-OJP, eruptions on that volcanically active LIP would be a plausible source.

2.2 Cismon core (Belluno Basin, Italy)

The Cismon core was drilled in the Southern Alps north-west of Treviso (Italy) in 1995, and is one of the best-studied latest Barremian–Aptian Tethyan records (Erba and Larson, 1998). The core largely consists of pale-coloured pelagic carbonates deposited on the slope of the Belluno Basin. However, the Selli Level Equivalent is marked by a clear lithological change to organic-rich marlstones and shales interbedded with sporadic radiolarian-rich beds (Erba and Larson, 1998). The increase in

TOC, together with elevated sulphur contents and preservation of the biomarker isorenieratane in some Selli Level Equivalent beds, strongly supports the development of at least periodically euxinic conditions in the Belluno Basin during OAE 1a (van Breugel *et al*., 2007; Bottini *et al*., 2012). Magneto-, bio-, and carbon-isotope stratigraphy provide excellent temporal constraints, with all the $\delta^{13}C$ excursions and C1–C8 segments well preserved (Menegatti *et al*., 1998; Erba *et al*., 1999; Channell *et al*., 2000). A pronounced decline in the abundance of nannoconids has been documented just below the Barremian–Aptian boundary, with a further reduction (to almost nothing) of these nannofossils near the base of the Selli Level Equivalent (Erba, 1994). These changes in the fossil record highlight the biotic impact of the environmental perturbations that took place prior to and during OAE 1a (e.g., Bralower *et al*., 1994; Erba, 1994; Erba and Tremolada, 2004; Erba *et al*., 2010). Age modelling of lower Aptian strata from the Cismon core have indicated dates for the Barremian–Aptian transition and OAE 1a that overlap with G-OJP basalt ages (see Malinverno *et al*., 2012; Erba *et al*., 2015). Furthermore, both osmium-isotope trends (see above) and enrichments in several trace metals of probable mafic derivation in Barremian–Aptian strata provide direct evidence of LIP activity at that time (Bottini *et al*., 2012; Erba *et al*., 2015).

2.3 Poggio le Guaine core (Umbria–Marche Basin, Italy)

The Poggio le Guaine (PLG) core was drilled in 2010 in the Northern Apennines at a site 6 km to the west of the city of Cagli (Coccioni *et al*., 2012), close to a previously studied lower Aptian outcrop that includes sediments of OAE 1a age deposited as the Selli Level *sensu stricto* (e.g., Lowrie *et al*., 1980; Coccioni *et al*., 1987, 1990; Baudin *et al*., 1998). Like the outcrop section, the core represents a well-preserved and apparently continuous Aptian–Albian succession that records a pelagic environment in the Umbria–Marche Basin of the north-western Tethyan area. The lithology is dominated by white and grey nannofossil-foraminiferal pelagic limestones, with rare cherts, radiolarian-rich beds, and green limestones (Coccioni *et al*., 2012; Savian *et al*., 2016). Stratigraphic age constraints on the position of the Barremian–Aptian boundary are based on magnetostratigraphy and calcareous planktonic

foraminiferal biostratigraphy (Coccioni *et al*., 2012; Savian *et al*., 2016). Intercalated organic-rich shales and radiolarian-rich beds, an overall relative elevation in TOC contents, and a negative (C3) and recovery/broad positive excursion (C4–C6) in carbonate $\delta^{13}C$ ratios all define the Selli Level (89.24–91.29 m; Coccioni *et al*., 2012; Savian *et al*., 2016; *this study*). However, within the OAE 1a strata there is a black-shale unit containing insufficient carbonate for carbon-isotope analysis, leaving a gap in the $\delta^{13}C$ trends that hinders precise placement of the C4–C5 and C5–C6 boundaries (~89–91 m).

2.4 Notre-Dame-de-Rosans (Vocontian Basin, SE France)

The Vocontian Basin was one of a number of large epicontinental depocentres located in the north-western area of the Cretaceous Tethys Ocean, formed by tectonic processes related to the opening of the Bay of Biscay (e.g., Hibsch *et al*., 1992), with basinal clay-rich calcareous hemipelagic sediments preserved today in south-eastern France (Bréhéret, 1997). The Notre-Dame-de-Rosans section provides an excellent record of OAE 1a in the Vocontian Basin, comprising interbedded clay-rich calcareous marls and fine-grained turbidites (Giraud *et al*., 2018). The stratigraphy can be correlated with other archives from that region, and elsewhere, based on biostratigraphic constraints, its carbon-isotope record (clearly documenting the C2–C7 segments), and the preservation of less calcareous, darker coloured, TOC-enriched grey marls in the upper part of the Selli Level Equivalent (Giraud *et al*., 2018), locally named the Niveau Goguel (Bréhéret, 1998). This organic matter is immature and appears to be largely composed of marine algal/bacterial material, but potentially with some contribution from degraded/terrestrially derived debris (Giraud *et al*., 2018). Based on the identification of <6 μm framboidal pyrite and cyanobacterial biomarkers in the Niveau Goguel strata of the nearby Les Sauzeries section (<50 km away), it has been inferred that anoxic–euxinic settings developed during the latter part of OAE 1a (Ando *et al*., 2013; Giraud *et al*., 2018). However, such conditions were likely intermittent, with the turbidite flows reventilating the marine environment (Caillaud *et al*., 2020).

2.5 DH-1 core, Longyearbyen (Boreal Basin, Svalbard, Norway)

The western part of Svalbard records a very near-shore shallow-marine palaeoenvironment in an epicontinental basin, with a lithology consisting of mudstone–siltstone beds, fluvial–marginal marine sandstone lenses, and coals (Midtkandal *et al*., 2016; Vickers *et al*., 2016). Macroscopic higher-plant debris in DH-1 core samples supports a dominantly terrestrial source of organic matter, further evidenced by low measured hydrogen index (HI) values, although the low HI could partly/completely result from the high thermal maturity of the sediments (Midtkandal *et al*., 2016). A limited quantity of marine palynomorphs allows for dinoflagellate biostratigraphy, from which a broadly Barremian–Aptian age for the interval of the DH-1 core studied here has been determined (Midtkandal *et al*., 2016). A negative $\delta^{13}C$ excursion and positive shift immediately stratigraphically above it (150.47–133.37 m) are thought to be equivalent to the C3 and C4–C6 segments, respectively, and have been interpreted as marking the Selli Level Equivalent strata in the core (Midtkandal *et al*., 2016). Further subdivision of the C4–C6 segments is not possible due to the low resolution of the $\delta^{13}C$ dataset. Interestingly, TOC contents decrease to an average of 1.8 wt% within the Selli Level Equivalent, compared to mean quantities of 3.8 wt% and 3.3. wt% in sediments stratigraphically above and below, respectively (Midtkandal *et al*., 2016). For this study, mercury analyses were limited to mudstone layers, avoiding sandstone/coal beds, in order to maintain relative consistency in terms of the lithology and organic-matter content of the studied samples, as previous works have shown that major lithological variations can strongly influence Hg concentrations and Hg/TOC variations independently of any potential external source (e.g., Percival *et al*., 2018).

2.6 Petrobras Well D (Sergipe-Alagoas Basin, NE Brazil)

The Sergipe-Alagoas Basin was one of a number of rift-basins along the eastern and southern part of Brazil that formed during the Early Cretaceous as a result of the opening of the South Atlantic

Ocean (Chaboureau *et al*., 2013, and references therein). The Petrobras Well D was drilled through the Muribeca and Riachuelo Formations of the basin, consisting of sandy and conglomeratic siliciclastics interbedded with siltstones and mudstones, the last of which are locally calcareous. Taken together, the stratigraphic sequence is interpreted as having been deposited in a continental–coastal setting that was initially dominated by fluvio-deltaic systems, but gradually transitioned towards lacustrine/lagoonal settings due to continuing basin subsidence as rifting of the South Atlantic proceeded (Tedeschi *et al*., 2020). Elsewhere in the Sergipe-Alagoas Basin, the Riachuelo Formation has been dated as late Aptian in age on the basis of planktonic foraminiferal biostratigraphy (e.g., Koutsoukos *et al*., 1992), with the underlying Muribeca Formation generally accepted as also having been deposited (earlier) in the Aptian (Tedeschi *et al*., 2020). Consequently, a series of pronounced carbon-isotope excursions near the bottom of the Muribeca Formation in the Petrobras Well D core has been interpreted as marking the Selli Level Equivalent, with a negative excursion overlain by two positive shifts interpreted as the C3 and C4–C6 segments, respectively (Tedeschi *et al*., 2020). TOC contents are variable, ranging from <0.1 wt% up to 5.2 wt%, with mean values highest in the postulated C5 strata, and primarily composed of detrital terrestrial organic matter that has locally been oxidized, based on the determined hydrogen and oxygen indices and the nature of the recorded palaeoenvironment (Tedeschi *et al*., 2020).

3. METHODS

Mercury data for all records were generated using a RA-915 Portable Mercury Analyzer with PYRO-915 Pyrolyzer, Lumex, at the University of Oxford (UK). Analyses were carried out following the methodology in Percival *et al*. (2017), with at least two analyses conducted for each sample. Two reference materials were utilized as standards for machine calibration and drift check throughout a set of analyses: NIMT/UOE/FM/001 – Inorganic Elements in Peat (169 ppb Hg) and NIST-SRM2587 – Trace Elements in Soil Containing Lead from Paint (290 ppb Hg). Analytical uncertainty based on repeated measurements of the reference materials was ±15 ppb. Concentrations of other metals in the DH-1 core samples were measured by ICP-AES at Imperial College London (UK) following

441 preparation by lithium metaborate fusion and hydrofluoric/perchloric acid digestion, after the methods
442 in Neumann *et al*. (2013).
443
444 New TOC data were generated by Rock-Eval 6 analysis for samples from DSDP Site 463, the
445 Cismon core, and Notre-Dame-de-Rosans, at the University of Oxford, after the methodology of Behar
446 *et al*. (2001). Repeated measurements of an internal mudrock standard SAB134 (calibrated to the
447 International reference material IFP 160000) were used to assess analytical accuracy and repeatability,
448 and yielded an average value of 2.81±0.07 wt%, consistent with long-term measurements for the
449 laboratory (2.87±0.11 wt%; Storm *et al*., 2020), and indicating analytical uncertainty better than 0.1
450 wt% (1σ). New TOC data for PLG core samples were determined on a Strohlein Coulomat 702 at the
451 University of Oxford, using the procedure in Jenkyns (1988). TOC contents have been previously
452 determined using Rock Eval and Leco SC-632 instruments for all samples from the DH-1 core and
453 Petrobras Well D analyzed for mercury in this study, at the Institute for Energy Technology, Kjeller
454 (Norway) for the DH-1 core (Midtkandal *et al*., 2016), and at the Universities of Oxford and
455 Universidade do Estado do Rio de Janeiro for Petrobras Well D (Tedeschi *et al*., 2020). The new data
456 from the Cismon core were combined with published values that were generated at the Open University
457 (UK) using a Leco CNS-2000 elemental analyser (Bottini *et al*., 2012).
458
459 New osmium-isotope data were determined for ten samples from the PLG core following the
460 methodology outlined in Kendall *et al*. (2015), with eight samples taken from the Selli Level, and two
461 others from beneath the base of it. Sample preparation utilized Carius-tube digestion with $Cr^{VI}O_3$-
462 H_2SO_4, with subsequent Os purification using established solvent extraction (by chloroform) and
463 microdistillation techniques (Selby and Creaser, 2003). Rhenium purification was carried out with
464 solvent extraction using sodium hydroxide and acetone, and subsequent anion exchange
465 chromatography (Cumming *et al*., 2013). Isotopic compositions and concentrations of rhenium and
466 osmium were determined by isotope dilution and negative thermal ionisation mass spectrometry (N-
467 TIMS) on a Thermo Triton instrument at the Department of Earth and Atmospheric Sciences, University
468 of Alberta (Canada). Total procedural blanks for osmium and rhenium were 0.3 and 15 pg, respectively,

whilst the $^{187}Os/^{188}Os$ composition of the blanks was 0.20. In-house standard solutions for osmium (AB2; see e.g., Selby, 2007; Finlay *et al*., 2010) and rhenium (ICP-MS standard rhenium solution of normal isotopic composition) yielded values in agreement with previous studies (van Acken *et al*., 2013; Kendall *et al*., 2015): $^{187}Os/^{188}Os$ of 0.10684±0.00015 (1σ) for osmium, and $^{185}Re/^{187}Re$ of 0.59778±0.00077 (1σ) for rhenium.

The past seawater composition at the time of deposition ($^{187}Os/^{188}Os_{(i)}$) is determined from the modern-day $^{187}Os/^{188}Os$ ratio of a sedimentary rock sample using its age and its Re and Os concentrations to account for the post-depositional decay of rhenium (^{187}Re) to ^{187}Os (Cohen *et al*., 1999). The osmium concentration of a sedimentary rock at the time of its deposition is determined from the modern-day osmium concentration after accounting for the post-depositional decay of ^{187}Re to ^{187}Os, by using the difference between the measured modern-day $^{187}Os/^{188}Os$ ratio and the calculated $^{187}Os/^{188}Os_{(i)}$ value, together with the ^{192}Os content of the rock and the known natural $^{192}Os/^{188}Os$ isotope ratio (see Supplementary Text).

4. RESULTS

4.1 Os-isotope and osmium concentration data from the PLG core

Following correction of the measured modern-day Os-isotope ratio for decay of rhenium since deposition at 120 Ma, the recorded $^{187}Os/^{188}Os_{(i)}$ values show a clear shift from ~0.6 to ~0.2 in the basal Selli Level strata (Figure 3). There is also a notable increase in the calculated [$Os_{(i)}$] concentrations across that horizon, from 149 ppt in the stratigraphically lowest analyzed sample to a maximum of 3719 ppt in the middle of the Selli Level. These trends are broadly consistent with osmium trends from Gorgo a Cerbara, Cismon (both Italy), DSDP Site 463 (Pacific), and Cau (Spain) reported by previous studies (Tejada *et al*., 2009; Bottini *et al*., 2012; Adloff *et al*., 2020). Interestingly, the transient shift to more

496 radiogenic $^{187}Os/^{188}Os_{(i)}$ values documented from other Tethyan records (Cismon and Gorgo a Cerbara;
497 Tejada *et al*., 2009; Bottini *et al*., 2012; see Figure 1) is not observed in the PLG data. This lack of
498 $^{187}Os/^{188}Os_{(i)}$ spike in the PLG core may result from the absence of data from below the Selli Level at
499 that site (Figure 3). Alternatively, the $^{187}Os/^{188}Os_{(i)}$ spike may not be captured by the PLG dataset due
500 to its relatively low-resolution, or the presence of a small hiatus/condensed layer at the base of the Selli
501 Level, although there is no sedimentological evidence for such a stratigraphic gap.
502
503
504 *4.2 Hg concentration and Hg/TOC ratio data*
505
506 At DSDP Site 463, there is a clear increase in Hg content from the average of 16.4 ppb below
507 the Selli Level Equivalent to a mean of 101 ppb within it, with a first increase up to 168.5 ppb in C3
508 (625.28–623.96 mbsf) and a second peak up to 471.5 ppb in the C4–lowest C5 segments (622.22–
509 620.10 mbsf), before returning to much lower (mean 18.4 ppb) values in sediments above the Selli
510 Level Equivalent (Figure 4A). By contrast, the TOC contents of DSDP Site 463 samples that were also
511 measured for mercury are relatively consistent, and low: typically <0.5 wt%, apart from for three
512 samples in the middle of the Selli Level Equivalent that have values close to or above 1 wt%.
513 Interestingly, no sample measured in this study had TOC contents of 7–8 wt% as reported for some
514 stratigraphic layers at DSDP Site 463 by previous works (see section 2.1). Consequently, the two
515 increases in Hg concentrations are largely reproduced by Hg/TOC ratios, with peaks up to 802 ppb/wt%
516 and 689 ppb/wt% in C3 and lowest C5 strata, respectively (Figure 4A). Crucially, both peaks greatly
517 exceed the range of error of background samples, confirming that they do not result from analytical
518 uncertainty. A small number of samples have a TOC content that is too low to confidently interpret
519 Hg/TOC ratios (Hg/TOC ratios based on TOC contents < 0.2 wt% are generally deemed unreliable due
520 to the high percentage error in the TOC measurement: see Grasby *et al*., 2016). However, the inclusion
521 or exclusion of these data does not greatly affect the recorded stratigraphic trends.
522

Hg concentrations in the Cismon core are extremely variable throughout the studied interval, ranging between 3.7–334 ppb with a number of peaks: either side of the Barremian–Aptian boundary (at 34.21 m and 27.85 m), within the C3 to C4 strata (~23 m), and again in the C6 segment between 19.87–18.83 m (Figure 4B). TOC contents of samples below the Selli Level Equivalent are typically very low (only three samples exceed 0.2 wt%), resulting in highly variable Hg/TOC values between 113–1637 ppb/wt% that also show peaks either side of the Barremian–Aptian boundary, although interpreting these data is greatly hindered due to the normalisation by extremely low TOC contents. By contrast, the typically higher TOC contents within the Selli Level Equivalent result in generally lower, though still variable, ratios between 7.9–468 ppb/wt% (Figure 4B). However, the C3–C4 peak in Hg concentrations is only reproduced by a two data-point peak in Hg/TOC, with no increase in Hg/TOC ratios in the C6 segment.

Similarly to the Cismon core, the PLG record features rather variable sedimentary Hg concentrations between 1.4–201 ppb, with a number of peaks below the Selli Level and another peak within the lower part of the C4–C6 strata within it (Figure 4C). Concentrations across the Barremian–Aptian boundary and above the Selli Level are particularly low (averaging 9.9 ppb). TOC contents increase markedly from typically <0.5 wt% below the Selli Level to values in excess of 2 wt% within it; one sample reaching 10.7 wt% (Figure 4C). The various peaks in Hg are maintained to some degree following normalisation against TOC, with three peaks of between 200–600 ppb/wt%: one at 93.8–93.6 m, a second at 92.2 m (both below the OAE 1a horizon), and finally at 90.4 m (lowest C4–C6 strata), albeit consisting of just one or two data points (Figure 4C). However, it should be noted that several PLG Hg data points are normalized against low (but >0.2 wt%) TOC contents, creating a high level of uncertainty in the Hg/TOC stratigraphic trend. Many of the PLG Hg/TOC peaks do not significantly exceed this range of error; thus, they cannot be unambiguously interpreted as marking an external influx of mercury.

Hg concentrations are consistently low through most of the Notre-Dame-de-Rosans strata (averaging 28.6 ppb), apart from a peak up to 156.5 ppb (mean 60.0 ppb) spanning the uppermost C3,

551 all of C4, and lower C5 segments (18.8–24.9 m; Figure 4D). Newly measured TOC contents in the
552 samples analyzed for mercury show comparable trends to those previously published by Giraud *et al*.
553 (2018), averaging approximately 0.5 wt% throughout most of the studied record, except in the C6 upper
554 part of the Selli Level Equivalent (the Niveau Goguel), where values rise to between 1–2 wt% (Figure
555 4D). Consequently, the peak in Hg concentrations largely remains following normalisation by TOC,
556 with an increase in Hg/TOC ratios up to 333 ppb/wt% in C4 strata, compared to consistently lower
557 values averaging 64 ppb/wt% throughout the rest of the studied interval.
558
559 Hg concentrations are variable throughout the studied interval of the DH-1 core, but show a
560 systematic increase across the Selli Level Equivalent. The basal (C3) strata are marked by a peak up to
561 202 ppb at 150.47 m, which is succeeded by a broader increase averaging 73.8 ppb across the upper
562 C4–C6 segments (144.3–136.02 m), compared to much lower contents that are typically <10 ppb
563 throughout the rest of the record (Figure 4E). When normalized against the TOC contents of these
564 samples (previously published by Midtkandal *et al*., 2016), the C3 peak in Hg largely disappears, but
565 the elevated Hg contents across C4–C6 strata are reflected by a rise in average Hg/TOC values to 40
566 ppb/wt% in these strata, compared to 12.1 ppb/wt% for the rest of the record (Figure 4E).
567
568 Hg concentrations are consistently very low (averaging 13.9 ppb) throughout the studied
569 interval of the Petrobras Well D, and show no increase across the postulated Selli Level Equivalent
570 (Figure 4F). As for the DH-1 core, TOC contents of these samples have been previously published
571 (Tedeschi *et al*., 2020), with a marked increase from <0.1 wt% below the OAE 1a level to generally
572 between 1–3 wt% (up to a maximum of 5.22 wt%) within it. Consequently, Hg/TOC ratios are generally
573 also very low (averaging <20 ppb/wt%) with a few higher values near the base of the studied interval
574 caused by low TOC contents (Figure 4F). There is one sample (from 201.43 m) with anomalously high
575 Hg concentrations and Hg/TOC ratios of 373 ppb and 158 ppb/wt%, respectively, but this is
576 significantly above the top of the Selli Level Equivalent.
577

5. DISCUSSION

5.1 Tethyan Hg-cycle disturbances prior to OAE 1a

Volcanic activity related to G-OJP emplacement has been previously proposed as having occurred during latest Barremian times, based on enrichments in mercury and other trace metals across the Barremian–Aptian boundary, especially in Tethyan stratigraphic archives (Erba *et al*., 2015; Charbonnier *et al*., 2018b). Some increase in submarine volcanism and/or basalt–seawater interaction might also be registered by a small shift towards mantle compositions in Pb and Os isotopes across the Barremian–Aptian boundaries of the Shatsky Rise and Cismon records, respectively (Kuroda *et al*., 2011; Bottini *et al*., 2012). It has been further suggested that this G-OJP volcanism contributed to the decline in nannoconid fauna during the Barremian–Aptian transition (Erba *et al*., 2015). Whilst Hg concentrations and Hg/TOC ratios are highly variable in pre-OAE 1a strata from the Cismon and PLG cores, peaks around the Barremian–Aptian boundary (and particularly strata of the magnetic chron CM0) might support a mercury-cycle disturbance in the Tethyan region at that time (Figure 4B–C). However, interpretation of the Hg/TOC ratios for both the Cismon and PLG cores is greatly hindered by the very low TOC contents of most samples (and attendant large range of uncertainty) from strata below the Selli Level or equivalent. Indeed, given the relatively low organic-matter and (in the case of Cismon) sulphur contents in Barremian–Aptian boundary sediments (Figure 4B–C; Supplementary Figure 2B), a lithological control on mercury deposition, whereby the element is associated with clay minerals, is likely for these strata. This conclusion is reinforced by the absence of Hg peaks in strata above the PLG Selli Level, when argillaceous layers (which make up much of the Selli Level and are interbedded with limestones beneath it) discontinue, leaving only calcareous lithologies.

Even if there were one or more Hg-cycle perturbations (volcanically stimulated or otherwise) in the Tethyan realm during the Barremian–Aptian transition prior to OAE 1a, there is no evidence that

605 such phenomena were occurring outside of this region. Hg concentrations and Hg/TOC ratios remain
606 relatively low throughout the (admittedly incomplete) strata below the Selli Level Equivalent at DSDP
607 Site 463 (Figure 4A). Given how proximal this Mid-Pacific Mountains site was to the G-OJP, if
608 volcanism on that LIP were capable of dispersing sufficient Hg to reach the northwest Tethys, the
609 expectation would be for it to be recorded in more proximal sedimentary records as well. Nor can the
610 absence of Barremian–Aptian Hg enrichment at DSDP Site 463 be attributed to overprinting by excess
611 TOC, as the Hg concentrations themselves largely remain low. Thus, whilst activity on the G-OJP
612 during the latest Barremian is not discounted as the cause of the nannoconid decline, if the LIP was
613 volcanically active at that time then it apparently did not perturb either the regional or global mercury
614 cycle significantly. Volcanism on the north-eastern Tethyan margin has been suggested as a potential
615 cause of Hg peaks in Valanginian sedimentary records from the northwest Tethys (Charbonnier *et al*.,
616 2017), but there is no clear indication that such eruptions took place during latest Barremian to early
617 Aptian times. Thus, without evidence of north-western Tethyan eruptions or G-OJP mercury emissions
618 during the Barremian–Aptian transition, the Hg/TOC variations documented stratigraphically below the
619 Selli Level (or equivalent strata) in the Cismon and PLG cores cannot be conclusively linked to
620 volcanism.
621
622
623 *5.2 Evidence for submarine G-OJP volcanism at the onset of OAE 1a*
624
625 The shift in $^{187}Os/^{188}Os_{(i)}$ values towards unradiogenic compositions in basal Selli Level (C3)
626 strata of the PLG core matches published Os-isotope stratigraphic trends from other sites in the Tethys
627 and Pacific (Figure 5). This similarity supports the commencement of intense LIP volcanism, or at least
628 some form of basalt–seawater interaction, during the onset of OAE 1a. There is a clear correlation
629 between the $^{187}Os/^{188}Os_{(i)}$ shift and the increased Hg and Hg/TOC values at DSDP Site 463; however,
630 no such relationship is documented in the Cismon or PLG cores (Figure 5). Whilst no $^{187}Os/^{188}Os_{(i)}$ data
631 exist for the other six sites studied for mercury here and by Charbonnier and Föllmi (2017), it can be
632 seen that although most of those locales record some enrichment(s) in sedimentary mercury, none of

633 them feature a clear peak in Hg and Hg/TOC in the C3 segment comparable to that in coeval strata of
634 DSDP Site 463 (Figure 4 and Supplementary Figure 1).
635
636 Given that by far the clearest sedimentary mercury enrichment during the onset of OAE 1a is
637 at DSDP Site 463, it is possible that this single-site peak results from a lithological change in that
638 archive, such as increased clay content or burial with pyrite (c.f., Shen *et al*., 2020). Alternatively, it
639 may reflect a local input of Hg from increased wildfire activity/runoff of terrestrial organic matter (c.f.
640 Daga *et al*., 2016; Grasby *et al*, 2017; Them *et al*., 2019). However, the C3 Hg enrichment at DSDP
641 Site 463 does not correlate with an increase in total clay or pyrite content (Supplementary Figure 2A),
642 ruling out an association between mercury and such phases, and thereby discounting lithological/redox
643 changes as the cause of the Hg/TOC increase. Organic-matter oxidation/degradation has been reported
644 from the DSDP Site 463 Aptian record, but van Breugel *et al*. (2007) noted that the sediments from the
645 basal part of the Selli Level Equivalent are less thermally mature than the rock layers stratigraphically
646 below and above, making it unlikely that the C3 Hg/TOC peak merely results from post-depositional
647 TOC depletion (c.f., Charbonnier *et al*., 2020). Both marine and terrestrially derived organic matter are
648 known to be present in Selli Level Equivalent sediments of DSDP Site 463, but an increased abundance
649 in terrestrial material specifically in the C3 Segment has not been robustly established (Mélières *et al*.
650 1981; Dean *et al*., 1984; van Breugel *et al*., 2007).
651
652 Notably, however, the Hg and Hg/TOC increase at the base of the Selli Level Equivalent
653 stratigraphically correlates with the appearance of abundant tuffaceous layers (Figure 6). Thus, it is
654 likely that the mercury peaks at DSDP Site 463 were caused by nearby volcanic activity proximal to
655 the G-OJP. The correlation between Hg enrichments, tuffaceous layers, and recorded shift in
656 $^{187}Os/^{188}Os_{(i)}$ ratios to unradiogenic compositions further suggests that all three could have been caused
657 by the same volcanic process. Given that the volcanic activity that caused the shift in seawater Os-
658 isotope ratio represented a six- to tenfold increase on pre-event background activity (Bauer *et al*., 2017),
659 it is highly unlikely that the volcanism responsible for the recorded Hg enrichment and $^{187}Os/^{188}Os_{(i)}$
660 shift at DSDP Site 463, which appears to have occurred at least proximally to the G-OJP, can have been

anything other than intense activity on that LIP. Moreover, given the intensity of this LIP volcanism, the fact that the mercury enrichment only appears in a site proximal to the G-OJP, and not correlative with $^{187}Os/^{188}Os_{(i)}$ shifts in the Tethyan realm, supports predominantly submarine eruptions, as also concluded by previous studies based on trends in other trace-element concentrations and lead-isotope signatures (Kuroda *et al*., 2011; Erba *et al*., 2015). The differing seawater residence times of osmium (10s kyr) and mercury (100s yr) would have enabled unradiogenic Os sourced from this volcanism to mix throughout the global ocean, whilst rapid Hg scavenging limited any evidence of a mercury flux to near the G-OJP, as documented in this study.

The slight possibility that the correlative Hg enrichment and $^{187}Os/^{188}Os_{(i)}$ shift at DSDP Site 463 were caused by HALIP volcanism is ruled out by the absence of a similar Hg peak in the C3 sediments of the Tethyan and (especially) DH-1 archives. It is possible that the one data-point Hg spike at the base of the C3 level in the DH-1 core represents a volcanic Hg flux from the HALIP that was then overprinted by excess TOC burial (as previously proposed for other sites by Percival *et al*., 2015, and Charbonnier and Föllmi, 2017), but this interpretation is speculative, and there is also no evidence for such an overprinting of increased Hg concentrations at any other site (Figure 4 and Supplementary Figure 1). If the HALIP had emitted sufficient mercury to the atmosphere to reach the Pacific, it is highly unlikely that there would be little clear record of such Hg output in any of the comparatively proximal Arctic or European/Tethyan sedimentary records (see Figure 2). Thus, the G-OJP is more likely to have been the primary source of mercury to the Mid-Pacific Mountains (and unradiogenic osmium to the global ocean as a whole).

Despite an apparent lack of impact on the Hg cycle, it cannot be excluded that the HALIP (as well as other carbon sources such as methane clathrates; e.g., Jahren *et al*., 2001) still contributed to causing the global C-cycle perturbation associated with OAE 1a. Such a scenario would likely have relied upon HALIP magmatic sills intruding organic-rich sediments with a low Hg content, causing massive emissions of isotopically light carbon, but little mercury output. However, it is not currently known whether such lithologies exist around the HALIP sills. Moreover, this scenario is at odds with

689 the documentation of Hg-cycle perturbations in stratigraphic records of several events linked with LIPs
690 thought to have featured thermogenic volatile emissions (e.g., Percival *et al*., 2015, 2017; Jones *et al*.,
691 2019; Shen *et al*., 2019b), and with preliminary investigations of carbon and mercury contents in shales
692 intruded by LIP magmas in South Africa, which show clear evidence for remobilisation of both volatiles
693 (Svensen *et al*., 2018). Therefore, it is more likely that the role played by the HALIP in initiating OAE
694 1a (if any) was minor compared to that of G-OJP activity.
695
696
697 *5.3 Volcanic* vs *terrestrial sources of Hg to marine environments after the onset of OAE 1a*
698
699 More plausibly, the widespread sedimentary Hg enrichments documented across C4 (or even
700 the very uppermost C3) to C5 strata of seven out of nine OAE 1a sites studied here and by Charbonnier
701 and Föllmi (2017) might have been triggered by a perturbation of the atmospheric mercury inventory
702 following emissions of the element to the atmosphere from one or both of HALIP volcanism and sill
703 intrusion of organic-rich shales. Given that subaerial LIP volcanism is thought to have emitted large
704 volumes of Hg to the atmosphere at other times in Earth's history (e.g., Sanei *et al*., 2012; Percival *et*
705 *al*., 2017, 2018; Grasby *et al*., 2019), similar eruptions on areas of the G-OJP that emerged above the
706 sea surface could also have produced this effect. However, because the C4–C5 strata postdate the onset
707 of OAE 1a by on the order of 10s kyr (Li *et al*., 2008; Malinverno *et al*., 2010), the sedimentary Hg
708 peaks might also result from lithological/redox changes or an increased input of terrigenous material
709 following environmental responses to the climate disruption associated with the event.
710
711 As outlined in section 1.3, mercury can be deposited in sediments bound to sulphides,
712 particularly in euxinic water columns (Shen *et al*., 2020). In this context, the fact that the Cismon core
713 records the development of euxinic conditions during OAE 1a (e.g., van Breugel *et al*., 2007), and that
714 C4 (and C6) strata from that archive marked by increased Hg concentrations also feature elevated
715 sulphur contents (Supplementary Figure 2B), may indicate a switch to mercury burial with sulphides in
716 the Belluno Basin during OAE 1a. If this association between Hg and S was the case, it could suggest

717 that redox changes and pyrite-deposition controlled sedimentary Hg contents at that location during
718 OAE 1a, rather than any external influx. And if so, it is likely that a similar situation existed for the
719 PLG core, given the similar palaeoenvironments and Hg/TOC records of the Cismon and PLG records
720 (only one or two high data points that do not exceed pre-event levels, or at least their range of
721 uncertainty). Whilst this local redox/sulphide control on mercury for these two sites remains unproven,
722 the relative paucity of high Hg/TOC values nonetheless means that robust evidence of a consistent
723 external flux of mercury to the Belluno and Umbria-Marche basins during OAE 1a is currently lacking.
724
725 However, C4–C5 strata, specifically, of Notre-Dame-de-Rosans, La Bédoule, Glaise, and
726 DSDP Site 463 record no evidence of euxinic conditions under which deposition of mercury with
727 sulphides would have been most likely (Mélières *et al*., 1981; van Breugel *et al*., 2007; Westermann *et*
728 *al*., 2013; Giraud *et al*., 2018), although DSDP Site 463 does feature an increased pyrite abundance in
729 the C4 segment (Mélières *et al*., 1981). Euxinic conditions are extremely unlikely to have developed in
730 the nearshore shallow-marine environment recorded by the DH-1 core, and a reasonably oxic (or at
731 least not severely anoxic) setting is supported for that record by low sedimentary molybdenum and
732 uranium concentrations, which show little or no enrichment above average-shale values except for two
733 samples above the Selli Level Equivalent (*this study*; see Supplementary Figure 2C). There is also no
734 correlation between the C4–C5 Hg enrichments and abundance of clays/Al_2O_3 at any of DSDP Site 463,
735 the DH-1 core, La Bédoule, or Glaise (see Supplementary Figure 2, and Charbonnier and Föllmi, 2017).
736 These trends support a lack of association between mercury and clay minerals in the C4–C5 strata at
737 those sites, which would be expected due to the abundant TOC content in these same sediments, given
738 the likely greater affiliation for mercury with organic matter over clays when both phases are present
739 (Shen *et al*., 2020). Thus, for at least four or five locations spanning the Arctic, Pacific, and north-
740 western Tethyan realms presented here and in Charbonnier and Föllmi (2017), there is no evidence that
741 mercury was deposited with a phase other than organic matter, making it likely that the C4–C5 peaks
742 in Hg and Hg/TOC values were caused by an increased influx of mercury rather than lithological/redox
743 changes.
744

745 Charcoal particles potentially indicative of wildfire activity have been reported from strata of
746 Aptian age (Brown *et al*., 2012; Wang *et al*., 2019), although not from the Selli Level Equivalent
747 specifically, or in any of the nine sites studied here and by Charbonnier and Föllmi (2017). Thus, there
748 is no positive evidence that the widespread Hg influxes were the result of wildfires, although such a
749 source cannot be completely ruled out. Nonetheless, terrestrially derived organic matter is abundant in
750 the DH-1 core, and is thought to be present in some mixture with marine material at all of DSDP Site
751 463, Notre-Dame-de-Rosans, and Glaise (van Breugel *et al*., 2007; Westermann *et al*., 2013;
752 Midtkandal *et al*. 2016; Giraud *et al*., 2018). Organic-matter contents are too low at La Bédoule to
753 reliably determine their composition. Thus, an increased input of terrigenous organic matter during a
754 time of increased riverine runoff is a theoretically plausible source of the mercury to these sites during
755 the early–middle part of OAE 1a, as previously proposed for the Early Jurassic Toarcian OAE (Them
756 *et al*., 2019). However, peak weathering rates during OAE 1a are thought to have been during C3 rather
757 than C4 (Tejada *et al*., 2009; Bottini *et al*., 2012; Lechler *et al*., 2015). Thus, if the mercury were derived
758 from runoff of terrestrial material, an enrichment would be expected in the C3 segment rather than C4–
759 C5 strata. Moreover, there is no evidence for an enhanced flux of mercury to the depositional setting of
760 the Petrobras Well D core, despite an increase in the content of terrestrially derived organic matter in
761 the upper part of the OAE 1a level (Tedeschi *et al*., 2020).
762
763 Consequently, whilst local terrestrial runoff cannot be discounted as the cause of the
764 widespread C4–C5 Hg-cycle perturbations, LIP-related emissions of mercury to the atmosphere provide
765 an equally plausible explanation. In the latter scenario, overprinting of Hg by excess TOC might have
766 muted any record of Hg/TOC peaks at sites such as Cismon or PLG (see Charbonnier and Föllmi, 2017).
767 As noted above, the lack of clear evidence of volcanic activity in the northwest Tethys during latest
768 Barremian to early Aptian times means that local eruptions cannot be unambiguously stated as the cause
769 of the observed C4–C5 Hg enrichments in Tethyan stratigraphic archives. Future studies incorporating
770 mercury-isotope analyses may aid determination of the pathways taken by the element to reach
771 depositional environments, and potentially indicate whether LIP activity or local processes such as

terrestrial runoff and/or wildfires were the main cause of the widespread Hg enrichments recorded in the C4–C5 segments (c.f., Grasby *et al*., 2017; Them *et al*., 2019).

5.4 Implications for the impact of magmatic CO_2 emissions from LIPs on the global carbon cycle

Even if the widespread Hg-cycle disturbances during the early–middle (C4–C5) part of OAE 1a were related to subaerial volcanism and/or HALIP-related thermogenic volatile emissions, this activity apparently did not commence until after the onset of the event. Thus, it is unlikely that these processes played a major role in triggering the crisis. Instead, the combined Hg enrichments at DSDP Site 463 and lack of clear C3 peaks from elsewhere strongly support submarine volcanism on the G-OJP as the dominant form of LIP activity during the onset of OAE 1a, suggesting magmatic CO_2 output from that province as the main driver of the carbon-cycle perturbations that initiated climate change. Such a scenario supports the model of Bauer *et al*. (2017) that G-OJP mantle-carbon emissions were sufficient to cause the pronounced negative CIE documented in C3 strata that record the onset of OAE 1a.

However, it remains unclear whether G-OJP volcanism caused a global carbon-cycle perturbation simply due to the huge volume ($59–77\times10^6$ km^3; Kerr and Mahoney, 2007), and high basaltic emplacement rate (possibly >100 km^3/yr; see introduction) of that LIP, particularly if it was combined with activity on the previously postulated twin province emplaced onto the Farallon Plate (Schlanger *et al*., 1981; Larson, 1991). If carbon emissions associated with the uniquely voluminous/rapid G-OJP magmatism were solely responsible for the negative CIE at the onset of OAE 1a, it would not detract from previous hypotheses that most (smaller) LIPs do not emit sufficient magmatic CO_2 to drive such disturbances unless combined with thermogenic volatiles and/or methane hydrate release (e.g., Hesselbo *et al*., 2000; Self *et al*., 2006). However, these results might also

highlight the possibility that all LIPs can drive such disturbances through magmatic carbon emissions alone (as previously hypothesized by e.g., Saunders, 2016; Gutjahr *et al*., 2017). Further studies of (intrusive and extrusive) LIP basalts and sediments intruded by magmatic sills, both for the G-OJP, HALIP and other provinces, are needed in order to constrain the potential outputs of different volatile species from magmatic and thermogenic sources, and to determine the extent to which these different sources could have perturbed the cycling of different elements at the Earth's surface during different geological periods.

6. CONCLUSIONS

This study has investigated the influence of different magmatic processes related to the development of large igneous provinces (LIPs) on the global environment, using OAE 1a as a case study. By combining new mercury data for six records of that event, including the first sites studied outside of the Tethyan realm, and new osmium-isotope evidence from one of these six (Poggio le Guaine) with previously published datasets, the types of LIP activity likely to have been most prevalent during the onset and main body of the event have been determined.

Although osmium-isotope trends are broadly consistent across all new and previously studied sites in documenting intense LIP activity throughout OAE 1a, records of mercury-cycle disturbance show considerable geographical variability. The only unambiguous Hg perturbation during the onset of OAE 1a (matching Os-isotope evidence of LIP activity) is recorded in the Mid-Pacific Mountains very proximal to the Greater Ontong-Java Plateau (G-OJP). No such clear evidence for mercury-cycle perturbations at that time is recorded at Tethyan or South Atlantic sites, or from the Arctic region proximal to the High Arctic Large Igneous Province (HALIP). This pattern supports G-OJP volcanism as the dominant form of LIP activity at the onset of OAE 1a, causing the globally documented Os-isotope shift but only localized Hg enrichment. These findings also re-emphasise previous hypotheses that oceanic LIPs only influence mercury cycling in immediately proximal regions, due to the limited

827 dispersal range of Hg emitted by submarine volcanism and other subaqueous basalt–seawater
828 interactions, and likely do not cause a global-scale perturbation.
829
830 Crucially, whilst submarine LIP activity on the G-OJP during the onset of OAE 1a is clearly
831 documented by osmium-isotope and mercury evidence, there is no clear indication for HALIP
832 magmatism at that time. More widespread, if generally less pronounced, mercury-cycle perturbations
833 appear to have taken place during the early–middle (C4–C5) part of OAE 1a. These disturbances could
834 have been linked to a transient pulse in subaerial eruptions or thermogenic emissions related to the
835 emplacement of the HALIP, or an intensification of/switch to subaerial eruptions on the G-OJP.
836 However, a non-volcanic cause of these widespread Hg-cycle disturbances after the onset of OAE 1a,
837 resulting from local environmental degradation during the event, cannot be ruled out. Even if these
838 widespread mercury enrichments do signify sub-aerial LIP activity, the observation that they are not
839 recorded globally in sediments that mark the onset of OAE 1a strongly suggests that such processes
840 could not have caused the event. Instead, the results appear to confirm that submarine volcanism active
841 on the Greater Ontong-Java Plateau, rather than sill intrusions of organic-rich sediments by the High
842 Arctic LIP, was likely the primary trigger for OAE 1a.
843
844
845 **ACKNOWLEDGEMENTS**
846
847 We greatly appreciate feedback from two anonymous reviewers that has improved this manuscript. We gratefully
848 acknowledge John Farmer and the University of Edinburgh for provision of geochemical standard material,
849 Stéphane Reboulet for fieldwork assistance at the Notre-Dame-de-Rosans section, and Steve Wyatt for aiding
850 laboratory analyses. The Poggio le Guaine (PLG) core drilling was financially supported by the Fundação de
851 Apoio à Universidade de São Paulo and Petrobras grant 2405. Peter Szatmari is thanked for conducting the
852 logistical arrangements required to perform rhenium-osmium analyses on PLG samples at the University of
853 Alberta. The UNIS CO2 Lab is thanked for providing access to the DH-1 core samples, and we greatly appreciate
854 assistance from Sverre Planke, Ivar Midtkandal, and Stéphane Polteau in sampling the core. We thank the UK

Natural Environment Research Council (NERC) grant NE/G01700X/1 (to Tamsin Mather), the European Research Council consolidator grant ERC-2018-COG-B18717-V-ECHO (to Tamsin Mather), NERC PhD studentship NE/L501530/1 (to Lawrence Percival), the Flanders Research Foundation (FWO) grant no. 12P4519N (to Lawrence Percival), the MIURPRIN (Ministero dell'Istruzione, dell'Università e della Ricerca–Progetti di Ricerca di Interesse Nazionale: grant no. PRIN 2017RX9XXXY to Elisabetta Erba), the Research Council of Norway Centres of Excellence (Project 223272 to Henrik Svensen), Petrobras (for financial support of the PLG and Petrobras Well D analyses and doctoral student funding for Leonardo R. Tedeschi), the Vrije Universiteit Brussel, and the Leverhulme Trust for funding.

REFERENCES

Adloff, M., Greene, S.E., Parkinson, I.J., Naafs, B.D.A., Preston, W., Ridgwell, A., Lunt, D.J., Castro, J.M. and Monteiro, F.M., 2020, Unravelling the sources of carbon emissions at the onset of Oceanic Anoxic Event (OAE) 1a. Earth and Planetary Science Letters, 530, 115947, https://doi.org/10.1016/j.epsl.2019.115947.

Allègre, C.J., Birck, J.L., Capmas, F. and Courtillot, V., 1999, Age of the Deccan traps using ^{187}Re–^{187}Os systematics. Earth and Planetary Science Letters, 170, p. 197–204, https://doi.org/10.1016/S0012-821X(99)00110-7.

Ando, A., Kaiho, K., Kawahata, H. and Kakegawa, T., 2008, Timing and magnitude of early Aptian extreme warming: Unraveling primary $\delta^{18}O$ variation in indurated pelagic carbonates at Deep Sea Drilling Project Site 463, central Pacific Ocean. Palaeogeography, Palaeoclimatology, Palaeoecology, 260, p. 463–476, https://doi.org/10.1016/j.palaeo.2007.12.007.

Ando, A., 2015, Intersite discrepancy in the amplitude of marine negative $\delta^{13}C$ excursion at the onset of early Aptian oceanic anoxic event 1a: Reconciliation through Sr isotopic screening of peculiar diagenetic overprint on the Pacific reference section (Deep Sea Drilling Project Site 463). *In* Neal, C.R., Sager, W.W., Sano, T. and Erba, E. (Eds.), The Origin, Evolution, and Environmental Impact of Oceanic

Large Igneous Provinces, Geological Society of America Special Paper, 511, p. 329–339, https://doi.org/10.1130/2015.2511(17).

Ando, T., Sawada, K., Takashima, R. and Nishi, H., 2013, Paleoproductivity of dinoflagellate and cyanobacteria during the mid-Cretaceous oceanic anoxic events in the Vocontian Basin, SE France. 26th IMOG Organic Geochemistry: Trends for the 21st Century, 2, p. 330–331.

Bagnato, E., Aiuppa, A., Parello, F., Calabrese, S., D'Alessandro, W., Mather**,** T.A., McGonigle, A.J.S., Pyle, D.M. and Wängberg, I., 2007, Degassing of gaseous (elemental and reactive) and particulate mercury from Mount Etna volcano (Southern Italy). Atmospheric Environment*,* 41, p.7377–7388, https://doi.org/10.1016/j.atmosenv.2007.05.060.

Baudin, F., Fiet, N., Coccioni, R. and Galeotti, S., 1998, Organic matter characterisation of the Selli Level (Umbria-Marche Basin, central Italy). Cretaceous Research, 19, p. 701–714, https://doi.org/10.1006/cres.1998.0126.

Bauer, K.W., Zeebe, R.E. and Wortmann, U.G., 2017, Quantifying the volcanic emissions which triggered Oceanic Anoxic Event 1a and their effect on ocean acidification. Sedimentology, 64, p. 204–214, https://doi.org/10.1111/sed.12335.

Behar, F., Beaumont, V. and de B. Penteado, H.L., 2001, Rock-Eval 6 technology: performances and developments. Oil & Gas Science and Technology, 56, p. 111–134, https://doi.org/10.2516/ogst:2001013.

Bond, D.P.G. and Wignall, P.B., 2014, Large igneous provinces and mass extinctions: an update. *In* Keller, G. and Kerr A.C. (Eds.), Volcnanism, Impacts, and Mass Extinctions: Causes and Effects, Geological Society of America Special Papers, 505, SPE505-02, https://doi.org/10.1130/2014.2505(02).

913 Bottini, C., Cohen, A.S., Erba, E., Jenkyns, H.C. and Coe, A.L., 2012, Osmium-isotope evidence for volcanism,
914 weathering, and ocean mixing during the early Aptian OAE 1a. Geology, 40, p. 583–586,
915 https://doi.org/10.1130/G33140.1.
916
917 Bottini, C., Erba, E., Tiraboschi, D., Jenkyns, H.C., Schouten, S. and Sinninghe Damsté, J.S., 2015, Climate
918 variability and ocean fertility during the Aptian Stage. Climate of the Past, 11, p. 383–402,
919 https://doi.org/10.5194/cp-11-383-2015.
920
921 Bowman, K.L., Hammerschmidt, C.R., Lamborg, C.H. and Swarr, G., 2015, Mercury in the North Atlantic Ocean:
922 The U.S. GEOTRACERS zonal and meridional sections. Deep-Sea Research II, 116, p. 251–261,
923 https://doi.org/10.1016/j.dsr2.2014.07.004.
924
925 Bralower, T.J., Arthur, M.A., Leckie, R.M., Sliter, W.V., Allard, D.J. and Schlanger, S.O., 1994, Timing and
926 paleoceanography of oceanic dysoxia/anoxia in the Late Barremian to Early Aptian (Early
927 Cretaceous). Palaios, p. 335–369, https://doi.org/10.2307/3515055.
928
929 Bréhéret, J.G., 1997, L'Aptien et l'Albien de la fosse vocontienne (des bordures au bassin): Evolution de la
930 sédimentation et enseignements sur les événements anoxiques. Société Géologique du Nord Publication
931 25, 614 p.
932
933 Bréhéret, J.G., 1998, Episodes de sédimentation riche en matière organique dans les marnes bleues d'âge aptien
934 et albien de la partie pélagique du bassin vocontien. Bulletin de la Société géologique de France, 4, p.
935 349–356, https://doi.org/10.2113/gssgfbull.IV.2.349.
936
937 Brown, S.A.E., Scott, A.C., Glasspool, I.J. and Collinson, M.E., 2012, Cretaceous wildfires and their impact on
938 the Earth system. Cretaceous research, 36, p. 162–190, https://doi.org/10.1016/j.cretres.2012.02.008.
939
940 Caillaud, A., Quijada, M., Huet, B., Reynaud, J.Y., Riboulleau, A., Bout-Roumazeilles, V., Baudin, F., Chappaz,
941 A., Adatte, T., Ferry, J.N. and Tribovillard, N., 2020, Turbidite-induced re-oxygenation episodes of the

sediment-water interface in a diverticulum of the Tethys Ocean during the Oceanic Anoxic Event 1a: The French Vocontian Basin. The Depositional Record, 6, p. 352–382, https://doi.org/10.1002/dep2.102.

Chaboureau, A.C., Guillocheau, F., Robin, C., Rohais, S., Moulin, M. and Aslanian, D., 2013, Paleogeographic evolution of the central segment of the South Atlantic during Early Cretaceous times: Paleotopographic and geodynamic implications. Tectonophysics, 604, p. 191–223, https://doi.org/10.1016/j.tecto.2012.08.025.

Chambers, L.M., Pringle, M.S. and Fitton, J.G., 2004, Phreatomagmatic eruptions on the Ontong Java Plateau: an Aptian $^{40}Ar/^{39}Ar$ age for volcaniclastic rocks at ODP Site 1184. *In* Fitton, J.G., Mahoney, J.J., Wallace, P.J. and Saunders, A.D. (Eds.), Origin and Evolution of the Ontong Java Plateau, Geological Society of London, Special Publications, 229, p. 325–331, https://doi.org/10.1144/GSL.SP.2004.229.01.18.

Channell, J.E.T., Erba, E., Muttoni, G. and Tremolada, F., 2000, Early Cretaceous magnetic stratigraphy in the APTICORE drill core and adjacent outcrop at Cismon (Southern Alps, Italy), and correlation to the proposed Barremian-Aptian boundary stratotype. Geological Society of America Bulletin, 112, p. 1430–1443, https://doi.org/10.1130/0016-7606(2000)112<1430:ECMSIT>2.0.CO;2.

Charbonnier, G. and Föllmi, K.B., 2017, Mercury enrichments in lower Aptian sediments support the link between Ontong Java large igneous province activity and oceanic anoxic episode 1a. Geology, 45, p. 63–66, https://doi.org/10.1130/G38207.1.

Charbonnier, G., Morales, C., Duchamp-Alphonse, S., Westermann, S., Adatte, T. and Föllmi, K.B., 2017, Mercury enrichment indicates volcanic triggering of Valanginian environmental change. Scientific reports, 7, https://doi.org/10.1038/srep40808.

Charbonnier, G., Adatte, T., Spangenberg, J.E. and Föllmi, K.B., 2018a, The expression of early Aptian to latest Cenomanian oceanic anoxic events in the sedimentary record of the Briançonnais domain. Global and planetary change, 170, p. 76–92, https://doi.org/10.1016/j.gloplacha.2018.08.009.

Charbonnier, G., Godet, A., Bodin, S., Adatte, T. and Föllmi, K.B., 2018b, Mercury anomalies, volcanic pulses, and drowning episodes along the northern Tethyan margin during the latest Hauterivian-earliest Aptian. Palaeogeography, Palaeoclimatology, Palaeoecology, 505, p. 337–350, https://doi.org/10.1016/j.palaeo.2018.06.013.

Charbonnier, G., Adatte, T., Föllmi, K.B. and Suan, G., 2020, Effect of intense weathering and post-depositional degradation of organic matter on Hg/TOC proxy in organic-rich sediments and its implications for deep-time investigations. Geochemistry, Geophysics, Geosystems, 21, https://doi.org/10.1029/2019GC008707.

Coccioni, R., Nesci, O., Tramontana, M., Wezel, F.C. and Moretti, E., 1987, Descrizione di un livello-guida "radiolaritico-bituminoso-ittiolitico" alla base delle Marne a Fucoidi nell'Appennino umbro-marchigiano. Bollettino della Società Geologica Italiana, 106, p. 183–192.

Coccioni, R., Franchi, R., Nesci, O., Perilli, N., Wezel, F.C. and Battistini, F., 1990, Stratigrafia, micropaleontologia e mineralogia delle Marne a Fucoidi delle sezioni di Poggio le Guaine e del Fiume Bosso (Appennino umbro-marchigiano). Atti 2° Convegno Internazionale "Fossili, Evoluzione, Ambiente", Pergola, 25-30 ottobre 1987. Tecnostampa, p. 163–201.

Coccioni, R., Jovane, L., Bancalà, G., Bucci, C., Fauth, G., Frontalini, F., Janikian, L., Savian, J., Paes de Almeida, R., Mathias, G.L. and Ferreira da Trindade, I.R., 2012, Umbria-Marche Basin, Central Italy: A reference section for the Aptian-Albian interval at low latitudes. Scientific Drilling, 13, p. 42–46, https://doi.org/10.2204/iodp.sd.13.07.2011.

Cogné, J.P. and Humler, E., 2006, Trends and rhythms in global seafloor generation rate. Geochemistry, Geophysics, Geosystems, 7, https://doi.org/10.1029/2005GC001148.

Cohen, A. S. and Coe, A. L., 2002, New geochemical evidence for the onset of volcanism in the Central Atlantic magmatic province and environmental change at the Triassic-Jurassic boundary. Geology, 30, p. 267–270, https://doi.org/10.1130/0091-7613(2002)030<0267:NGEFTO>2.0.CO;2.

Cohen, A.S., Coe, A.L., Bartlett, J.M. and Hawkesworth, C.J., 1999, Precise Re-Os ages of organic-rich mudrocks and the Os isotope composition of Jurassic seawater. Earth and Planetary Science Letters, 167, p. 159–173, https://doi.org/10.1016/S0012-821X(99)00026-6.

Corfu, F., Polteau, S., Planke, S., Faleide, J.I., Svensen, H., Zayoncheck, A. and Stolbov, N., 2013, U–Pb geochronology of Cretaceous magmatism on Svalbard and Franz Josef Land, Barents Sea large igneous province. Geological Magazine, 150, p. 1127–1135, https://doi.org/10.1017/S0016756813000162.

Cumming, V.M., Poulton, S.W., Rooney, A.D. and Selby, D., 2013, Anoxia in the terrestrial environment during the late Mesoproterozoic. Geology, 41, p. 583–586, https://doi.org/10.1130/G34299.1.

Daga, R., Guevara, S.R., Pavlin, M., Rizzo, A., Lojen, S., Vreča, P., Horvat, M. and Arribére, M., 2016, Historical records of mercury in southern latitudes over 1600 years: Lake Futalaufquen, Northern Patagonia. Science of the Total Environment, 553, p. 541–550, https://doi.org/10.1016/j.scitotenv.2016.02.114.

Dean, W.E., Claypool, G.E. and Thide, J., 1984, Accumulation of organic matter in Cretaceous oxygen-deficient depositional environments in the central Pacific Ocean. Organic geochemistry, 7, p. 39–51, https://doi.org/10.1016/0146-6380(84)90135-9.

Dickson, A.J., Cohen, A.S., Coe, A.L., Davies, M., Shcherbinina, E.A. and Gavrilov, Y.O., 2015, Evidence for weathering and volcanism during the PETM from Arctic and Peri-Tethys osmium isotope records. Palaeogeography, Palaeoclimatology, Palaeoecology, 438, p. 300–307, https://doi.org/10.1016/j.palaeo.2015.08.019.

Dockman, D.M., Pearson, D.G., Heaman, L.M., Gibson, S.A. and Sarkar, C., 2018, Timing and origin of magmatism in the Sverdrup Basin, Northern Canada—Implications for lithospheric evolution in the High Arctic Large Igneous Province (HALIP). Tectonophysics, 742, p. 50–65, https://doi.org/10.1016/j.tecto.2018.05.010.

Dumitrescu M. and Brassell S.C., 2006, Compositional and isotopic characteristics of organic matter for the early Aptian Oceanic Anoxic Event at Shatsky Rise, ODP Leg 198. Palaeogeography, Palaeoclimatolology, Palaeoecology, 235, p. 168–191, https://doi.org/10.1016/j.palaeo.2005.09.028.

Erba, E., 1994, Nannofossils and superplumes: the early Aptian "nannoconid crisis". Paleoceanography and Paleoclimatology, 9, p. 483–501, https://doi.org/10.1029/94PA00258.

Erba, E., 2004, Calcareous nannofossils and Mesozoic oceanic anoxic events. Marine micropaleontology, 52, p. 85–106, https://doi.org/10.1016/j.marmicro.2004.04.007.

Erba, E. and Larson, R.L., 1998, The Cismon APTICORE (Southern Alps, Italy): a" reference section" for the Lower Cretaceous at low latitudes. Rivista Italiana di Paleontologia e Stratigrafia (Research In Paleontology and Stratigraphy), 104, p. 181–192.

Erba, E. and Tremolada, F., 2004, Nannofossil carbonate fluxes during the Early Cretaceous: Phytoplankton response to nutrification episodes, atmospheric CO_2, and anoxia. Paleoceanography, 19, https://doi.org/10.1029/2003PA000884.

Erba, E., Channell, J.E.T., Claps, M., Jones, C., Larson, R., Opdyke, B., Premoli Silva, I., Riva, A., Salvini, G. and Torricelli, S., 1999, Integrated stratigraphy of the Cismon Apticore (southern Alps, Italy); a "reference section" for the Barremian-Aptian interval at low latitudes. Journal of Foraminiferal Research, 29, p. 371–391.

Erba, E., Bottini, C., Weissert, H.J. and Keller, C.E., 2010, Calcareous nannoplankton response to surface-water acidification around Oceanic Anoxic Event 1a. Science, 329, p. 428–432, https://doi.org/10.1126/science.1188886.

Erba, E., Duncan, R.A., Bottini, C., Tiraboschi, D., Weissert, H., Jenkyns, H.C. and Malinverno, A., 2015, Environmental consequences of Ontong Java Plateau and Kerguelen Plateau volcanism. *In* Neal, C.R.,

Sager, W.W., Sano, T. and Erba, E. (Eds.), The Origin, Evolution, and Environmental Impact of Oceanic Large Igneous Provinces, Geological Society of America Special Paper, 511, p. 271–303, https://doi.org/10.1130/2015.2511(15).

Ericksen, J.A., Gustin, M.S., Schorran, D.E., Johnson, D.W., Lindberg, S.E. and Coleman, J.S., 2003, Accumulation of atmospheric mercury in forest foliage. Atmospheric Environment, 36, p. 1613–1622, https://doi.org/10.1016/S1352-2310(03)00008-6.

Finlay, A.J., Selby, D. and Gröcke, D.R., 2010, Tracking the Hirnantian glaciation using Os isotopes. Earth and Planetary Science Letters, 293, p. 339–348, https://doi.org/10.1016/j.epsl.2010.02.049.

Föllmi, K.B., Godet, A., Bodin, S. and Linder, P., 2006, Interactions between environmental change and shallow water carbonate buildup along the northern Tethyan margin and their impact on the Early Cretaceous carbon isotope record. Paleoceanography, 21, https://doi.org/10.1029/2006PA001313.

Gales, E., Black, B. and Elkins-Tanton, L.T., 2020, Carbonatites as a record of the carbon isotope composition of large igneous province outgassing. Earth and Planetary Science Letters, 535, 116076, https://doi.org/10.1016/j.epsl.2020.116076.

Giraud, F., Pittet, B., Grosheny, D., Baudin, F., Lécuyer, C. and Sakamoto, T., 2018, The palaeoceanographic crisis of the Early Aptian (OAE 1a) in the Vocontian Basin (SE France). Palaeogeography, Palaeoclimatology, Palaeoecology, 511, p. 483–505, https://doi.org/10.1016/j.palaeo.2018.09.014.

Gladczenko, T.P., Coffin, M.F. and Eldholm, O., 1997, Crustal structure of the Ontong Java Plateau: modeling of new gravity and existing seismic data. Journal of Geophysical Research: Solid Earth, 102, p. 22711–22729, https://doi.org/10.1029/97JB01636.

Grasby, S.E., Beauchamp, B., Bond, D.P.G., Wignall, P.B. and Sanei, H., 2016, Mercury anomalies associated with three extinction events (Capitanian crisis, latest Permian extinction and the Smithian/Spathian

extinction) in NW Pangea. Geological Magazine, 153, p. 285–297, https://doi.org/10.1017/S0016756815000436.

Grasby, S.E., Wenjie, S., Runsheng, Y., Gleason, J.D., Blum, J.D., Lepak, R.F., Hurley, J.P. and Beauchamp, B., 2017, Isotopic signatures of mercury contamination in latest Permian oceans. Geology, 45, p. 55–58, https://doi.org/10.1130/G38487.1.

Grasby, S.E., Them, T.R., Chen, Z., Yin, R. and Ardakani, O.H., 2019, Mercury as a proxy for volcanic emissions in the geologic record. Earth-Science Reviews, 196, 102880 https://doi.org/10.1016/j.earscirev.2019.102880.

Gröcke, D.R., Hesselbo, S.P. and Jenkyns, H.C., 1999, Carbon-isotope composition of Lower Cretaceous fossil wood: Ocean-atmosphere chemistry and relation to sea-level change. Geology, 27, p. 155–158, https://doi.org/10.1130/0091-7613(1999)027<0155:CICOLC>2.3.CO;2.

Gutjahr, M., Ridgwell, A., Sexton, P.F., Anagnostou, E., Pearson, P.N., Pälike, H., Norris, R.D., Thomas, E. and Foster, G.L., 2017, Very large release of mostly volcanic carbon during the Palaeocene–Eocene Thermal Maximum. Nature, 548, p. 573–577, https://doi.org/10.1038/nature23646.

Hammer, Ø., Jones, M.T., Schneebeli-Hermann, E., Hansen, B.B. and Bucher, H., 2019, Are Early Triassic extinction events associated with mercury anomalies? A reassessment of the Smithian/Spathian boundary extinction. Earth-Science Reviews, 195, p. 179–190, https://doi.org/10.1016/j.earscirev.2019.04.016.

Hein, J.R. and Vanek, E., 1981, Origin and alteration of volcanic ash and pelagic brown clay, Deep Sea Drilling Project Leg 62, north-central Pacific. Initial Reports of the Deep Sea Drilling Project, 62, p. 559–569 https://doi.org/10.2973/dsdp.proc.62.120.1981.

Hesselbo, S.P., Gröcke, D.R., Jenkyns, H.C., Bjerrum, C.J., Farrimond, P., Morgans-Bell, H.S. and Green, O.R., 2000, Massive dissociation of gas hydrate during a Jurassic oceanic anoxic event. Nature, 406, p. 392–395, https://doi.org/10.1038/35019044.

Hibsch, C., Jandel, D., Montenat, C. and Ott d'Estevou, P., 1992, Evénements tectoniques crétacés dans la partie méridionale du bassin subalpin (massif Ventoux-Lure et partie orientale de l'arc de Castellane, SE France). Implications géodynamiques. Bulletin de la Société Géologique de France, 163, p. 147–158.

Hoernle, K., Hauff, F., van den Bogaard, P., Werner, R., Mortimer, N., Geldmacher, J., Garbe-Schönberg, D. and Davy, B., 2010, Age and geochemistry of volcanic rocks from the Hikurangi and Manihiki oceanic Plateaus. Geochimica et Cosmochimica Acta, 74, p. 7196–7219, https://doi.org/10.1016/j.gca.2010.09.030.

Hönisch, B., Ridgwell, A., Schmidt, D.N., Thomas, E., Gibbs, S.J., Sluijs, A., Zeebe, R., Kump, L., Martindale, R.C., Greene, S.E., Kiessling, W., Ries, J., Zachos, J.C., Royer, D.L., Barker, S., Marchitto, T.M., Moyer, R., Pelejero, C., Ziveri, P., Foster, G.L. and Williams, B., 2012, The geological record of ocean acidification. Science, 335, p. 1058–1063, https://doi.org/10.1126/science.1208277.

Hu, X., Zhao, K., Yilmaz, I.O. and Li, Y., 2012, Stratigraphic transition and palaeoenvironmental changes from the Aptian oceanic anoxic event 1a (OAE1a) to the oceanic red bed 1 (ORB1) in the Yenicesihlar section, central Turkey. Cretaceous Research, 38, p. 40–51, https://doi.org/10.1016/j.cretres.2012.01.007.

Jahren, A.H., Arens, N.C., Sarmiento, G., Guerrero, J. and Amundson, R., 2001, Terrestrial record of methane hydrate dissociation in the Early Cretaceous. Geology, 29, p. 159–162, https://doi.org/10.1130/0091-7613(2001)029<0159:TROMHD>2.0.CO;2.

Jenkyns, H.C., 1988, The early Toarcian (Jurassic) anoxic event: Stratigraphic, sedimentary, and geochemical evidence. American Journal of Science, 288, p. 101–151, https://doi.org/10.2475/ajs.288.2.101.

Jenkyns, H.C., 1995, Carbon-isotope stratigraphy and paleoceanographic significance of the Lower Cretaceous shallow-water carbonates of Resolution Guyot, Mid-Pacific Mountains. *In* Winterer, E.L., Sager, W.W., Firth, J.V. and Sinton J.M. (Eds.), Proceedings of the Ocean Drilling Program, Scientific Results, 143,

p. 99–104. College Station, Texas, Ocean Drilling Program, https://doi.org/10.2973/odp.proc.sr.143.213.1995.

Jenkyns, H.C., 2010, Geochemistry of oceanic anoxic events. Geochemistry, Geophysics, Geosystems, 11, https://doi.org/10.1029/2009GC002788.

Jenkyns, H.C., 2018, Transient cooling episodes during Cretaceous Oceanic Anoxic Events with special reference to OAE 1a (Early Aptian). Philosophical Transactions of the Royal Society A: Mathematical, Physical and Engineering Sciences, 376, 20170073, https://doi.org/10.1098/rsta.2017.0073.

Jones, C.E. and Jenkyns, H.C., 2001, Seawater strontium isotopes, oceanic anoxic events, and seafloor hydrothermal activity in the Jurassic and Cretaceous. American Journal of Science, 301, p. 112–149, https://doi.org/10.2475/ajs.301.2.112.

Jones, M.T., Percival, L.M.E., Stokke, E.W., Frieling, J., Mather, T.A., Riber, L., Schubert, B.A., Schultz, B., Tegner, C., Planke, S. and Svensen H., 2019, Mercury anomalies across the Palaeocene–Eocene Thermal Maximum. Climate of the Past, 15, p. 217–236, https://doi.org/10.5194/cp-15-217-2019.

Kendall, B., Creaser, R.A., Reinhard, C.T., Lyons, T.W. and Anbar, A.D., 2015, Transient episodes of mild environmental oxygenation and oxidative continental weathering during the late Archean. Science Advances, 1, e1500777, https://doi.org/10.1126/sciadv.1500777.

Kerr, A.C. and Mahoney, J.J., 2007, Oceanic plateaus: Problematic plumes, potential paradigms. Chemical Geology, 241, p. 332–353, https://doi.org/10.1016/j.chemgeo.2007.01.019.

Kongchum, M., Hudnall, W.H. and Delaune, R.D., 2011, Relationship between sediment clay minerals and total mercury. Journal of Environmental Science and Health, Part A, 46, p. 534–539, https://doi.org/10.1080/10934529.2011.551745.

Koutsoukos, E.A.M., 1992, Late Aptian to Maastrichtian foraminiferal biogeography and palaeoceanography of the Sergipe Basin, Brazil. Palaeogeography, palaeoclimatology, palaeoecology, 92, p. 295–324, https://doi.org/10.1016/0031-0182(92)90089-N.

Kuhnt, W., Holbourn, A. and Moullade, M., 2011, Transient global cooling at the onset of early Aptian oceanic anoxic event (OAE) 1a. Geology, 39, p. 323–326, https://doi.org/10.1130/G31554.1.

Kuroda, J., Tanimizu, M., Hori, R.S., Suzuki, K., Ogawa, N.O., Tejada, M.L.G., Coffin, M.F., Coccioni, R., Erba, E. and Ohkouchi, N., 2011, Lead isotopic record of Barremian–Aptian marine sediments: Implications for large igneous provinces and the Aptian climatic crisis. Earth and Planetary Science Letters, 307, p. 126–134, https://doi.org/10.1016/j.epsl.2011.04.021.

Larson, R.L., 1991, Latest pulse of Earth: Evidence for a mid-Cretaceous superplume. Geology, 19, p. 547–550, https://doi.org/10.1130/0091-7613(1991)019<0547:LPOEEF>2.3.CO;2.

Larson, R.L. and Erba, E., 1999, Onset of the Mid-Cretaceous greenhouse in the Barremian-Aptian: Igneous events and the biological, sedimentary, and geochemical responses. Paleoceanography, 14, https://doi.org/10.1029/1999PA900040.

Lechler, M., Pogge von Strandmann, P.A.E., Jenkyns, H.C., Prosser, G. and Parente, M., 2015, Lithium-isotope evidence for enhanced silicate weathering during OAE 1a (Early Aptian Selli event). Earth and Planetary Science Letters, 432, p. 210–222, https://doi.org/10.1016/j.epsl.2015.09.052.

Li, Y.X., Bralower, T.J., Montañez, I.P., Osleger, D.A., Arthur, M.A., Bice, D.M., Herbert, T.D., Erba, E. and Silva, I.P., 2008, Toward an orbital chronology for the early Aptian Oceanic Anoxic Event (OAE1a, ~120 Ma). Earth and Planetary Science Letters, 271, p. 88–100, https://doi.org/10.1016/j.epsl.2008.03.055.

1207 Lowrie, W., Alvarez, W., Silva, I.P. and Monechi, S., 1980, Lower Cretaceous magnetic stratigraphy in Umbrian
1208 pelagic carbonate rocks. Geophysical Journal International, 60, p. 263–281,
1209 https://doi.org/10.1111/j.1365-246X.1980.tb04292.x.
1210
1211 Malinverno, A., Erba, E. and Herbert, T.D., 2010, Orbital tuning as an inverse problem: Chronology of the early
1212 Aptian oceanic anoxic event 1a (Selli Level) in the Cismon APTICORE. Paleoceanography and
1213 Paleoclimatology, 25, https://doi.org/10.1029/2009PA001769.
1214
1215 McElwain, J.C., Wade-Murphy, J. and Hesselbo, S.P., 2005, Changes in carbon dioxide during an oceanic anoxic
1216 event linked to intrusion into Gondwana coals. Nature, 435, p. 479–482,
1217 https://doi.org/10.1038/nature03618.
1218
1219 Méhay, S., Keller, C.E., Bernasconi, S.M., Weissert, H., Erba, E., Bottini, C. and Hochuli, P.A., 2009, A volcanic
1220 CO_2 pulse triggered the Cretaceous Oceanic Anoxic Event 1a and a biocalcification crisis. Geology, 37,
1221 p. 819–822, https://doi.org/10.1130/G30100A.1.
1222
1223 Mélières, F., Deroo, G. and Herbin, J.P., 1981, Organic-matter-rich and hypersiliceous Aptian sediments from
1224 western Mid-Pacific Mountains. Initial Reports of the Deep Sea Drilling Project, 62, p. 903–915,
1225 https://doi.org/10.2973/dsdp.proc.62.146.1981.
1226
1227 Menegatti, A.P., Weissert, H., Brown, R.S., Tyson, R.V., Farrimond, P., Strasser, A. and Caron, M., 1998, High-
1228 resolution $\delta^{13}C$ stratigraphy through the early Aptian "Livello Selli" of the Alpine
1229 Tethys. Paleoceanography, 13, https://doi.org/10.1029/98PA01793.
1230
1231 Midtkandal, I., Svensen, H., Planke, S., Corfu, F., Polteau, S., Torsvik, T.H., Faleide, J.I., Grundvåg, S.A., Selnes,
1232 H., Kürschner, W. and Olaussen, S., 2016, The Aptian (Early Cretaceous) oceanic anoxic event (OAE1a)
1233 in Svalbard, Barents Sea, and the absolute age of the Barremian-Aptian boundary. Palaeogeography,
1234 Palaeoclimatology, Palaeoecology, 463, p. 126–135, https://doi.org/10.1016/j.palaeo.2016.09.023.
1235

1236 Mutterlose, J., Bottini, C., Schouten, S. and Sinninghe Damsté, J.S., 2014, High sea-surface temperatures during
1237 the early Aptian Oceanic Anoxic Event 1a in the Boreal Realm. Geology, 42, p. 439–442,
1238 https://doi.org/10.1130/G35394.1.
1239
1240 Naafs, B.D.A. and Pancost, R.D., 2016, Sea-surface temperature evolution across Aptian Oceanic Anoxic Event
1241 1a. Geology, 44, p. 959–962, https://doi.org/10.1130/G38575.1.
1242
1243 Naafs, B.D.A., Castro, J.M., De Gea, G.A., Quijano, M.L., Schmidt, D.N. and Pancost, R.D., 2016, Gradual and
1244 sustained carbon dioxide release during Aptian Oceanic Anoxic Event 1a. Nature Geoscience, 9, p. 135–
1245 139, https://doi.org/10.1038/ngeo2627.
1246
1247 Neumann, E.R., Svensen, H., Tegner, C., Planke, S., Thirlwall, M. and Jarvis, K.E., 2013, Sill and lava
1248 geochemistry of the mid-Norway and NE Greenland conjugate margins. Geochemistry, Geophysics,
1249 Geosystems, 14, https://doi.org/10.1002/ggge.20224.
1250
1251 Pancost, R.D., Crawford, N., Magness, S., Turner, A., Jenkyns, H.C. and Maxwell, J.R., 2004, Further evidence
1252 for the development of photic-zone euxinic conditions during Mesozoic oceanic anoxic events. Journal
1253 of the Geological Society, 161, p. 353–364, https://doi.org/10.1144/0016764903-059.
1254
1255 Paquay, F.S. and Ravizza, G., 2012, Heterogeneous seawater $^{187}Os/^{188}Os$ during the late Pleistocene
1256 glaciations. Earth and Planetary Science Letters, 349, p. 126–138,
1257 https://doi.org/10.1016/j.epsl.2012.06.051.
1258
1259 Percival, L.M.E., Witt, M.L.I., Mather, T.A., Hermoso, M., Jenkyns, H.C., Hesselbo, S.P., Al-Suwaidi, A.H.,
1260 Storm, M.S., Xu, W. and Ruhl, M., 2015, Globally enhanced mercury deposition during the end-
1261 Pliensbachian extinction and Toarcian OAE: A link to the Karoo–Ferrar Large Igneous Province. Earth
1262 and Planetary Science Letters, 428, p. 267–280, https://doi.org/10.1016/j.epsl.2015.06.064.
1263
1264 Percival, L.M.E., Ruhl, M., Hesselbo, S.P., Jenkyns, H.C., Mather, T.M. and Whiteside, J.H., 2017, Mercury
1265 evidence for pulsed volcanism during the end-Triassic mass extinction. Proceedings of the National

Academy of Sciences of the United States of America, 114, p. 7929–7934, https://doi.org/10.1073/pnas.1705378114.

Percival, L.M.E., Jenkyns, H.C., Mather, T.A., Dickson, A.J., Batenburg, S.J., Ruhl, M., Hesselbo, S.P., Barclay, R., Jarvis, I., Robinson, S.A., Woelders, L., 2018, Does Large Igneous Province volcanism always perturb the mercury cycle? Comparing the records of Oceanic Anoxic Event 2 and the end-Cretaceous to other Mesozoic events. American Journal of Science, 318 p. 799–860, https://doi.org/10.2475/08.2018.01.

Percival, L.M.E., Bergquist, B.A., Mather, T.A. and Sanei, H., 2021, Sedimentary mercury enrichments as a tracer of Large Igneous Province volcanism. In Ernst, R.E., Dickson, A.J., Bekker, A. (Eds.): Large Igneous Provinces: A Driver of Global Environmental and Biotic Change. AGU Geophysical Monograph, 255, p. 247–262, https://doi.org/10.1002/9781119507444.ch11.

Peucker-Ehrenbrink, B. and Jahn, B.M., 2001, Rhenium-osmium isotope systematics and platinum group element concentrations: Loess and the upper continental crust. Geochemistry, Geophysics, Geosystems, 2, https://doi.org/10.1029/2001GC000172.

Peucker-Ehrenbrink, B. and Ravizza, G., 2000, The marine osmium isotope record. Terra Nova, 12, p. 205–219, https://doi.org/10.1046/j.1365-3121.2000.00295.x.

Polteau, S., Hendriks, B.W.H., Planke, S., Ganerød, M., Corfu, F., Faleide, J.I., Midtkandal, I., Svensen, H. and Kyklebust, R., 2016, The Early Cretaceous Barents Sea Sill Complex: Distribution, $^{40}Ar/^{39}Ar$ geochronology, and implications for carbon gas formation. Palaeogeography, Palaeoclimatology, Palaeoecology, 441, p. 83–95, https://doi.org/10.1016/j.palaeo.2015.07.007.

Price, G.D., 2003, New constraints upon isotope variation during the early Cretaceous (Barremian–Cenomanian) from the Pacific Ocean. Geological Magazine, 140, p. 513–522, https://doi.org/10.1017/S0016756803008100.

Pyle, D.M., and Mather, T.A., 2003, The importance of volcanic emissions for the global atmospheric mercury cycle. Atmospheric Environment, 37, p. 5115–5124, https://doi.org/10.1016/j.atmosenv.2003.07.011.

Robinson, S.A., Clarke, L.J., Nederbragt, A. and Wood, I.G., 2008, Mid-Cretaceous oceanic anoxic events in the Pacific Ocean revealed by carbon-isotope stratigraphy of the Calera Limestone, California, USA. Geological Society of America Bulletin, 120, p. 1416–1426, https://doi.org/10.1130/B26350.1.

Robinson, S.A., Heimhofer, U., Hesselbo, S.P. and Petrizzo, M.R., 2017, Mesozoic climates and oceans – a tribute to Hugh Jenkyns and Helmut Weissert. Sedimentology, 64, p. 1–15, https://doi.org/10.1111/sed.12349.

Sanei, H., Grasby, S.E. and Beauchamp, B., 2012, Latest Permian mercury anomalies. Geology, 40, p. 63–66, https://doi.org/10.1130/G32596.1.

Saunders, A.D., 2016, Two LIPs and two Earth-system crises: the impact of the North Atlantic Igneous Province and the Siberian Traps on the Earth-surface carbon cycle. Geological Magazine, 153, p. 201–222, https://doi.org/10.1017/S0016756815000175.

Savian, J., Trindade, R., Janikian, L., Jovane, L., de Almeida, R.P., Coccioni, R., Frontalini, F., Sideri, M., Figueiredo, M., Tedeschi, L.R. and Jenkyns, H.C., 2016, The Barremian-Aptian boundary in the Poggio le Guaine core (central Italy): Evidence for magnetic polarity Chron M0r and oceanic anoxic event 1a. *In* Menichetti, M., Coccioni, R. and Montanari, A. (Eds.), The Stratigraphic Record of Gubbio: Integrated Stratigraphy of the Late Cretaceous–Paleogene Umbria-Marche Pelagic Basin, Geological Society of America Special Paper, 524, p. 57–78, https://doi.org/10.1130/2016.2524(05).

Scaife, J.D., Ruhl, M., Dickson, A.J., Mather, T.A., Jenkyns, H.C., Percival, L.M.E., Hesselbo, S.P., Cartwright, J., Eldrett, J.S., Bergman, S.C. and Minisini, D., 2017, Sedimentary Mercury Enrichments as a Marker for Submarine Large Igneous Province Volcanism? Evidence from the Mid-Cenomanian Event and Oceanic Anoxic Event 2 (Late Cretaceous). Geochemistry, Geophysics, Geosystems, 18, https://doi.org/10.1002/2017GC007153.

Schoene, B., Eddy, M.P., Samperton, K.M., Keller, C.B., Keller, G., Adatte, T. and Khadri, S.F.R., 2019. U-Pb constraints on pulsed eruption of the Deccan Traps across the end-Cretaceous mass extinction. Science, 363, p. 862–866, https://doi.org/10.1126/science.aau2422.

Schroeder, W.H. and Munthe J., 1998, Atmospheric mercury - An overview. Atmospheric Environment, 32, p. 809–822, https://doi.org/10.1016/S1352-2310(97)00293-8.

Schlanger, S.O. and Jenkyns, H.C., 1976, Cretaceous oceanic anoxic events: causes and consequences. Geologie en Mijnbouw, 55, p. 179–184.

Schlanger, S.O., Jenkyns, H.C. and Premoli-Silva, I., 1981, Volcanism and vertical tectonics in the Pacific Basin related to global Cretaceous transgressions. Earth and Planetary Science Letters, 52, p. 435-449, https://doi.org/10.1016/0012-821X(81)90196-5.

Selby, D., 2007, Direct Rhenium-Osmium age of the Oxfordian-Kimmeridgian boundary, Staffin bay, Isle of Skye, UK, and the Late Jurassic time scale. Norwegian Journal of Geology, 87, p. 291–299.

Selby, D. and Creaser, R.A., 2003, Re–Os geochronology of organic rich sediments: an evaluation of organic matter analysis methods. Chemical Geology, 200, p. 225–240, https://doi.org/10.1016/S0009-2541(03)00199-2.

Self, S., Widdowson, M., Thordarson, T. and Jay, A.E., 2006, Volatile fluxes during flood basalt eruptions and potential effects on the global environment: A Deccan perspective. Earth and Planetary Science Letters, 248, p. 518–532, https://doi.org/10.1016/j.epsl.2006.05.041.

Selin, N.E., 2009, Global Biogeochemical Cycling of Mercury: A Review. Annual Review of Environment and Resources, 34, p. 43–63, https://doi.org/10.1146/annurev.environ.051308.084314.

Shen, J., Algeo, T.J., Chen, J., Planavsky, N.J., Feng, Q., Yu, J. and Liu, J., 2019a, Mercury in marine Ordovician/Silurian boundary sections of South China is sulfide-hosted and non-volcanic in origin. Earth and Planetary Science Letters, 511, p. 130–140, https://doi.org/10.1016/j.epsl.2019.01.028.

Shen, J., Chen, J., Algeo, T.J., Yuan, S., Feng, Q., Yu, J., Zhou, L., O`Connell, B., Planavsky, N.J., 2019b, Evidence for a prolonged Permian–Triassic extinction interval from global marine mercury records. Nature Communications, 10, https://doi.org/10.1038/s41467-019-09620-0.

Shen, J., Feng, Q., Algeo, T.J., Liu, J., Zhou, C., Wei, W., Liu, J., Them II, T.R., Gill, B.C. and Chen, J., 2020, Sedimentary host phases of mercury (Hg) and implications for use of Hg as a volcanic proxy. Earth and Planetary Science Letters, 543, 116333, https://doi.org/10.1016/j.epsl.2020.116333.

Sliter, W.V., 1989, Aptian anoxia in the Pacific Basin. Geology, 17, p. 909–912, https://doi.org/10.1130/0091-7613(1989)017<0909:AAITPB>2.3.CO;2.

Storm, M.S., Hesselbo, S.P., Jenkyns, H.C., Ruhl, M., Ullmann, C.V., Xu, W., Leng, M.J., Riding, J.B. and Gorbanenko, O., 2020, Orbital pacing and secular evolution of the Early Jurassic carbon cycle. Proceedings of the National Academy of Sciences of the United States of America, 117, p. 3974–3982, https://doi.org/10.1073/pnas.1912094117.

Svensen, H., Planke, S., Malthe-Sørenssen, A., Jamtveit, B., Myklebust, R., Eidem, T.R. and Rey, S.S., 2004, Release of methane from a volcanic basin as a mechanism for initial Eocene global warming. Nature, 429, p. 542–545, https://doi.org/10.1038/nature02566.

Svensen, H., Percival, L.M.E., Jones, M.T. and Mather, T.A., 2018, Release of mercury from black shale during contact metamorphism and the implications for mercury as a volcanic proxy. Geophysical Research Abstracts, 20, EGU2018-10291-1, EGU General Assembly.

Tarduno, J.A., Sliter, W.V., Bralower, T.J., McWilliams, M., Premoli-Silva, I. and Ogg, J.G., 1989, M-sequence reversals recorded in DSDP sediment cores from the western Mid-Pacific Mountains and Magellan

Rise. Geological Society of America Bulletin, 101, p. 1306–1316, https://doi.org/10.1130/0016-7606(1989)101<1306:MSRRID>2.3.CO;2.

Taylor, B., 2006, The single largest oceanic plateau: Ontong Java–Manihiki–Hikurangi. Earth and Planetary Science Letters, 241, p. 372–380, https://doi.org/10.1016/j.epsl.2005.11.049.

Tedeschi, L.R., Jenkyns, H.C., Robinson, S.A., Lana, C.C., Menezes Santos, M.R.F. and Tognoli, F.M., 2020, Aptian carbon-isotope record from the Sergipe-Alagoas Basin: New insights into oceanic anoxic event 1a and the timing of seawater entry into the South Atlantic. Newsletters on Stratigraphy, 53, p. 333–364, https://doi.org/10.1127/nos/2019/0529.

Tegner, C., Storey, M., Holm, P.M., Thorarinsson, S.B., Zhao, X., Lo, C.H. and Knudsen, M.F., 2011, Magmatism and Eurekan deformation in the High Arctic Large Igneous Province: ^{40}Ar-^{39}Ar age of Kap Washington Group volcanics. North Greenland. Earth and Planetary Science Letters, 303, p. 203–214, https://doi.org/10.1016/j.epsl.2010.12.047.

Tejada, M. L. G., Suzuki, K., Kuroda, J., Coccioni, R., Mahoney, J. J., Ohkouchi, N., Sakamoto, T. and Tatsumi, Y., 2009, Ontong Java Plateau eruption as a trigger for the early Aptian oceanic anoxic event. Geology, 37, p. 855–858, https://doi.org/10.1130/G25763A.1.

Them, T.R., Jagoe, C.H., Caruthers, A.H., Gill, B.C., Grasby, S.E., Gröcke, D.R., Yin, R. and Owens, J.D., 2019, Terrestrial sources as the primary delivery mechanism of mercury to the oceans across the Toarcian Oceanic Anoxic Event (Early Jurassic). Earth and Planetary Science Letters, 507, p. 62–72, https://doi.org/10.1016/j.epsl.2018.11.029.

Thiede, J. *et al*., 1981, Site 463: Western Mid-Pacific Mountains. Initial Reports of the Deep Sea Drilling Project, 62, p. 33–156, https://doi.org/10.2973/dsdp.proc.62.102.1981.

1412 Thiede, J., Dean, W.E., and Claypool, G.E., 1982, Oxygen-deficient depositional paleoenvironments in the mid-
1413 Cretaceous tropical and sub-tropical central Pacific Ocean. *In* Schlanger, S.O., and Cita, M.B. (Eds.),
1414 Nature and origin of Cretaceous carbon-rich facies: London, Academic Press, p. 79–100.
1415
1416 Thordarson, T., 2004, Accretionary-lapilli-bearing pyroclastic rocks at ODP Leg 192 Site 1184: a record of
1417 subaerial phreatomagmatic eruptions on the Ontong Java Plateau. *In* Fitton, J.G., Mahoney, J.J., Wallace,
1418 P.J. and Saunders, A.D. (Eds.), Origin and Evolution of the Ontong Java Plateau, Geological Society of
1419 London, Special Publications, 229, p. 275–306, https://doi.org/10.1144/GSL.SP.2004.229.01.16.
1420
1421 Turgeon, S.C. and Creaser, R.A., 2008. Cretaceous oceanic anoxic event 2 triggered by a massive magmatic
1422 episode. Nature, 454, p. 323–326, https://doi.org/10.1038/nature07076.
1423
1424 Vallier, T.L. and Jefferson, W.S., 1981, Volcanogenic Sediments from Hess Rise and the Mid-Pacific Mountains,
1425 Deep Sea Drilling Project Leg 62. *In* Thiede, J. and Vallier, T.L. *et al.*, Initial Reports of the Deep Sea
1426 Drilling Project, 62, p. 545–557, https://doi.org/10.2973/dsdp.proc.62.119.1981.
1427
1428 van Acken, D., Thomson, D., Rainbird, R.H. and Creaser, R.A., 2013, Constraining the depositional history of
1429 the Neoproterozoic Shaler Supergroup, Amundsen Basin, NW Canada: Rhenium-osmium dating of black
1430 shales from the Wynniatt and Boot Inlet Formations. Precambrian Research, 236, p. 124–131,
1431 https://doi.org/10.1016/j.precamres.2013.07.012.
1432
1433 van Breugel, Y., Schouten, S., Tsikos, H., Erba, E., Price, G.D. and Sinninghe Damsté, J.S., 2007, Synchronous
1434 negative carbon isotope shifts in marine and terrestrial biomarkers at the onset of the early Aptian oceanic
1435 anoxic event 1a: Evidence for the release of ^{13}C-depleted carbon into the
1436 atmosphere. Paleoceanography, 22, https://doi.org/10.1029/2006PA001341.
1437
1438 Vickers, M.L., Price, G.D., Jerrett, R.M. and Watkinson, M., 2016, Stratigraphic and geochemical expression of
1439 Barremian–Aptian global climate change in Arctic Svalbard. Geosphere, 12, p. 1594–1605,
1440 https://doi.org/10.1130/GES01344.1.
1441

Wang, S., Shao, L.Y., Yan, Z.M., Shi, M.J. and Zhang, Y.H., 2019, Characteristics of Early Cretaceous wildfires in peat-forming environment, NE China. Journal of Palaeogeography, 8, https://doi.org/10.1186/s42501-019-0035-5.

Weissert, H., 1989, C-isotope stratigraphy, a monitor of paleoenvironmental change: a case study from the Early Cretaceous. Surveys in Geophysics, 10, p. 1–61, https://doi.org/10.1007/BF01901664.

Westermann, S., Stein, M., Matera, V., Fiet, N., Fleitmann, D., Adatte, T. and Föllmi, K.B., 2013, Rapid changes in the redox conditions of the western Tethys Ocean during the early Aptian oceanic anoxic event. Geochimica et Cosmochimica Acta, 121, p. 467–486, https://doi.org/10.1016/j.gca.2013.07.023.

FIGURE CAPTIONS

Figure 1: Previously published trends across the Selli Level Equivalent of the Cismon core for **A)** carbon isotopes and **B)** osmium isotopes and osmium concentrations (data from Erba *et al*., 1999; Bottini *et al*., 2012). The grey shaded area indicates the stratigraphic extent of Selli Level Equivalent sediments deposited during OAE 1a; the dashed grey line the Barremian–Aptian boundary at the base of magnetozone M0 (Erba *et al*., 1999; Channell *et al*., 2000; Bottini *et al*., 2012). The stratigraphic levels of both the decline and crisis of nannoconids (Erba *et al*., 1999) are indicated by thin dashed black lines, and the $\delta^{13}C$ segments (from Menegatti *et al*., 1998) by solid thin black lines. See methods section for details on the calculation of initial seawater Os-isotope ratios ($^{187}Os/^{188}Os_{(i)}$) and sedimentary osmium concentrations ($[Os_{(i)}]$). Lithology, biostratigraphy, magnetostratigraphy, and carbon-isotope segments are sourced as for Figure 4.

Figure 2: Palaeogeographic map of the Barremian–Aptian world (~120 Ma). The positions of the HALIP and G-OJP are indicated by dark red areas. Locations A–F mark sites of sedimentary records investigated for mercury in this study (black squares = mercury and osmium-isotope data presented; black circles = mercury data presented). Locations G–I (black triangles) indicate sites previously studied for mercury

by Charbonnier and Föllmi (2017). Global map is adapted from van Breugel *et al*. (2007), with the western Tethys inset adapted from Giraud *et al*. (2018).

Figure 3: Stratigraphic correlation of $\delta^{13}C$ ratios, and recorded $^{187}Os/^{188}Os_{(i)}$ and $[Os_{(i)}]$ values at 120 Ma for the Poggio le Guaine (PLG) core. Stratigraphic scale is in metres. $\delta^{13}C$ values, biostratigraphy, and carbon-isotope segments are sourced as for Figure 4; all osmium data are from this study. Grey shaded area indicates the stratigraphic extent of the Selli Level.

Figure 4: Geochemical data plots for $\delta^{13}C$, TOC, Hg contents, and Hg/TOC ratios for DSDP Site 463, the Cismon core, Poggio le Guaine (PLG) core, Notre-Dame-de-Rosans, the DH-1 core, and Petrobras Well D. Semi-transparent Hg/TOC data points indicate Hg/TOC ratios based on TOC contents <0.2 wt% (below the limit of reliability recommended by Grasby *et al.*, 2016). The ±15 ppb range of Hg concentration uncertainty is indicated on each Hg data plot by a pale red field; the 0.1 wt% uncertainty on TOC measurements is not visible on this scale. The uncertainty range for each Hg/TOC value based on ±15 ppb Hg and ±0.1 wt% TOC is shown on each Hg/TOC plot by a pale red field. Grey shaded areas indicate the stratigraphic extent of the Selli Level (at PLG) or equivalent strata deposited during OAE 1a (all other sites), the grey dashed line the Barremian–Aptian boundary, and thin black dashed lines the recorded decline and crisis of nannoconids. All stratigraphic scales are in metres. All Hg and Hg/TOC data are new for this study. TOC data are sourced as follows: the DSDP Site 463, Poggio le Guaine core and Notre-Dame-de-Rosans from this study; the Cismon core from Bottini *et al*. (2012) and this study; the DH-1 core from Midtkandal *et al*. (2016); Petrobras Well D from Tedeschi *et al.* (2020). $\delta^{13}C$ data and information on lithology, biostratigraphy, magnetostratigraphy, and carbon-isotope segmentation are sourced as follows: DSDP Site 463 from Tarduno *et al*. (1989), Erba (1994), Bottini *et al*. (2012), and Ando *et al*. (2015); the Cismon core from Menegatti *et al*. (1998), Erba *et al*. (1999), Channell *et al*. (2000); the Poggio le Guaine core from Savian *et al*. (2016); Notre-Dame-de-Rosans from Giraud *et al*. (2018); DH-1 core from Midtkandal *et al*. (2016); Petrobras Well D from Tedeschi *et al.* (2020). Previously published TOC data for DSDP Site 463 and Notre-Dame-de-Rosans that were not used for normalisation of Hg are sourced from Bottini *et al*. (2012) and Giraud *et al*. (2018), respectively. The $\delta^{13}C$ and Hg data from DSDP Site 463 and the Cismon and DH-1 cores are presented alongside evidence for clay and pyrite/sulphur contents in Supplementary Figure 2.

Figure 5: Stratigraphic correlation of Hg/TOC ratios and $^{187}Os/^{188}Os_{(i)}$ trends from DSDP Site 463 and the Cismon and Poggio le Guaine (PLG) cores. Semi-transparent Hg/TOC data points indicate Hg/TOC ratios based on TOC contents <0.2 wt% (below the limit of reliability recommended by Grasby *et al*., 2016). The uncertainty range for each Hg/TOC value based on ±15 ppb Hg and ±0.1 wt% TOC is shown by the pale red field. Published Os data from DSDP Site 463 and the Cismon core are from Bottini *et al*. (2012); Poggio le Guaine Os data and all Hg data are from this study. Grey shaded areas indicate the stratigraphic extent of the Selli Level or equivalent OAE 1a strata, the grey dashed line the Barremian–Aptian boundary, and thin black dashed lines the recorded decline and crisis of nannoconids. All stratigraphic scales are in metres. Information on lithology, $\delta^{13}C$ values, biostratigraphy, magnetostratigraphy, and carbon-isotope segments are sourced as for Figure 4.

Figure 6: Stratigraphic correlation of mercury concentrations, Hg/TOC ratios, and recorded $^{187}Os/^{188}Os_{(i)}$ and $[Os_{(i)}]$ values at 120 Ma for DSDP Site 463. Semi-transparent Hg/TOC data points indicate Hg/TOC ratios based on TOC contents <0.2 wt% (below the limit of reliability recommended by Grasby *et al*., 2016). Yellow lines mark the stratigraphic positions of tuffaceous layers (Thiede *et al*., 1981). The grey shaded area indicates the stratigraphic extent of Selli Level Equivalent sediments deposited during OAE 1a, the grey dashed line the Barremian–Aptian boundary, and thin black dashed lines the recorded decline and crisis of nannoconids. All stratigraphic scales are in metres. Information on lithology, $\delta^{13}C$ values, biostratigraphy, magnetostratigraphy, and carbon-isotope segments are sourced as for Figure 4. The uncertainty range for each Hg and Hg/TOC value based on ±15 ppb Hg and ±0.1 wt% TOC are shown by the pale red field on their respective data plots.

Figure 1

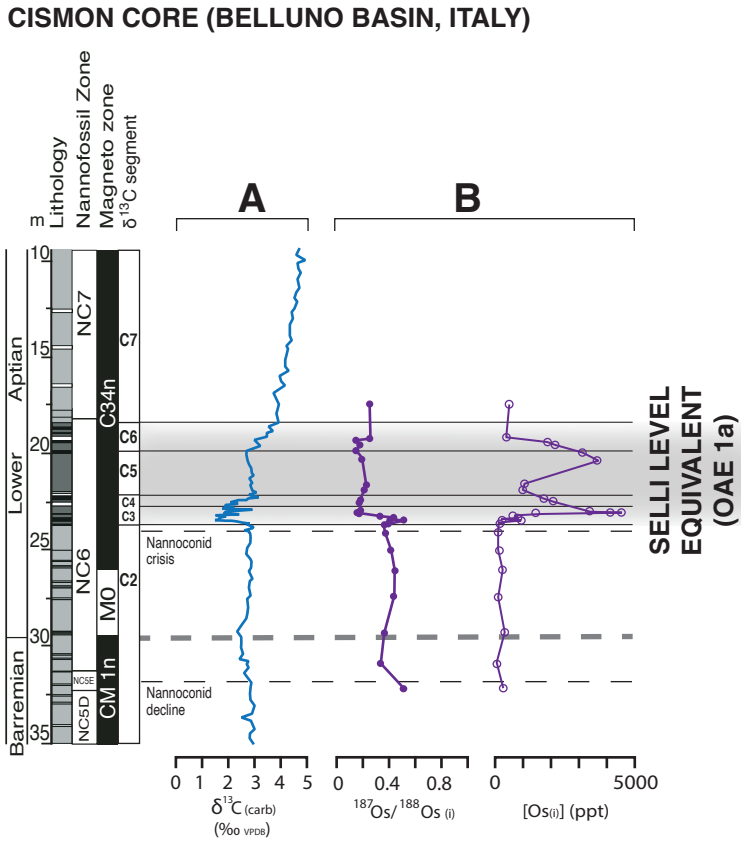
CISMON CORE (BELLUNO BASIN, ITALY)
m
Lithology
Nannofossil Zone
Magneto zone
δ13C segment
A
B
10
15
20
25
30
35
Aptian
Lower
Barremian
NC7
NC6
NC5E
NC5D
C34n
M0
CM 1n
C7
C6
C5
C4
C3
C2
Nannoconid crisis
Nannoconid decline
SELLI LEVEL EQUIVALENT (OAE 1a)
0 1 2 3 4 5
δ13C (carb) (‰ VPDB)
0 0.4 0.8
187Os/188Os (i)
0 5000
[Os(i)] (ppt)

Figure 2

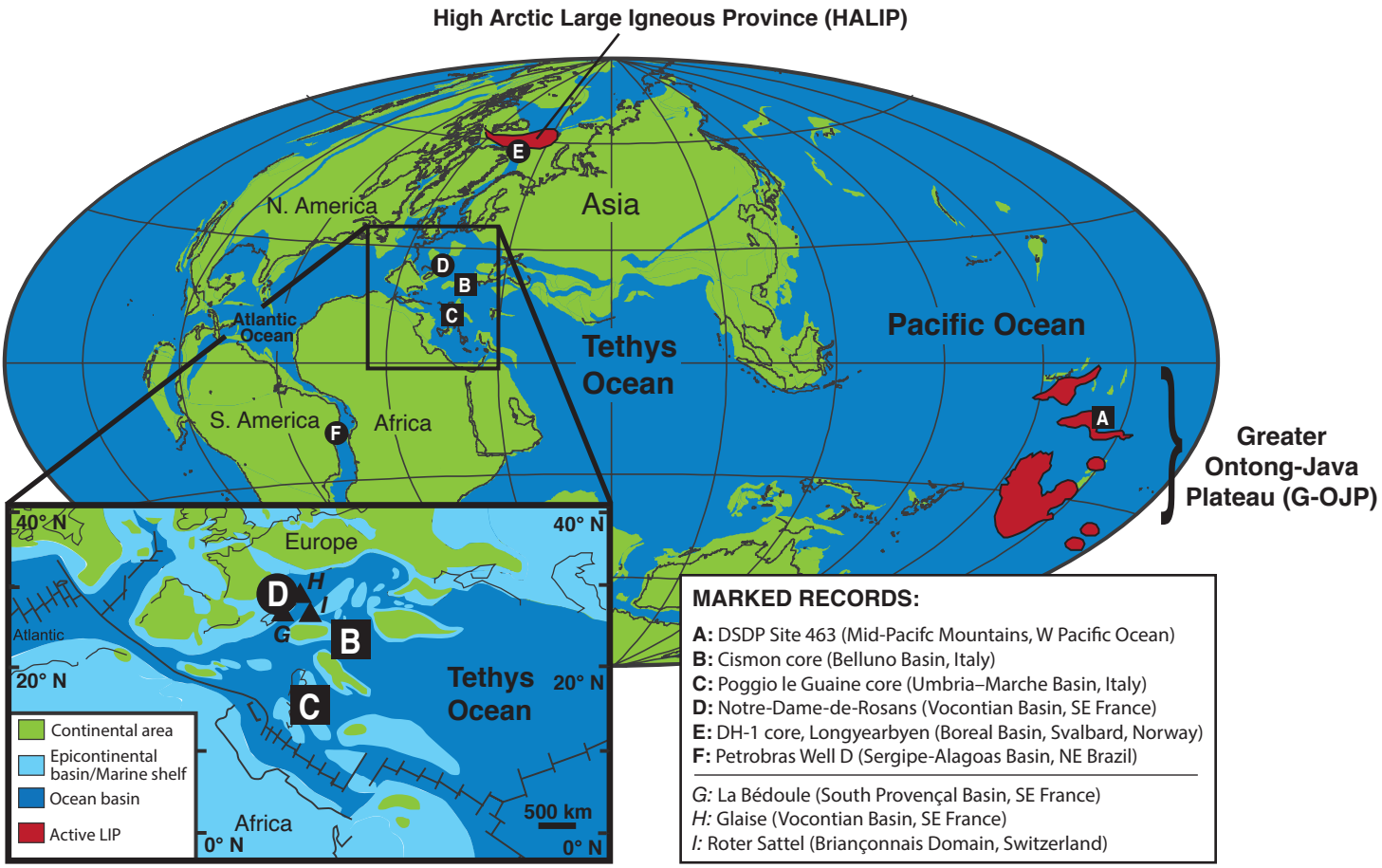
BARREMIAN–APTIAN PALAEOGEOGRAPHY (~120 Ma)
High Arctic Large Igneous Province (HALIP)
N. America
Asia
Atlantic Ocean
Tethys Ocean
Pacific Ocean
S. America
Africa
Greater Ontong-Java Plateau (G-OJP)
40° N
Europe
Atlantic
20° N
Tethys Ocean
Continental area
Epicontinental basin/Marine shelf
Ocean basin
Active LIP
500 km
0° N
MARKED RECORDS:
A: DSDP Site 463 (Mid-Pacifc Mountains, W Pacific Ocean)
B: Cismon core (Belluno Basin, Italy)
C: Poggio le Guaine core (Umbria–Marche Basin, Italy)
D: Notre-Dame-de-Rosans (Vocontian Basin, SE France)
E: DH-1 core, Longyearbyen (Boreal Basin, Svalbard, Norway)
F: Petrobras Well D (Sergipe-Alagoas Basin, NE Brazil)
G: La Bédoule (South Provençal Basin, SE France)
H: Glaise (Vocontian Basin, SE France)
I: Roter Sattel (Briançonnais Domain, Switzerland)

Figure 3

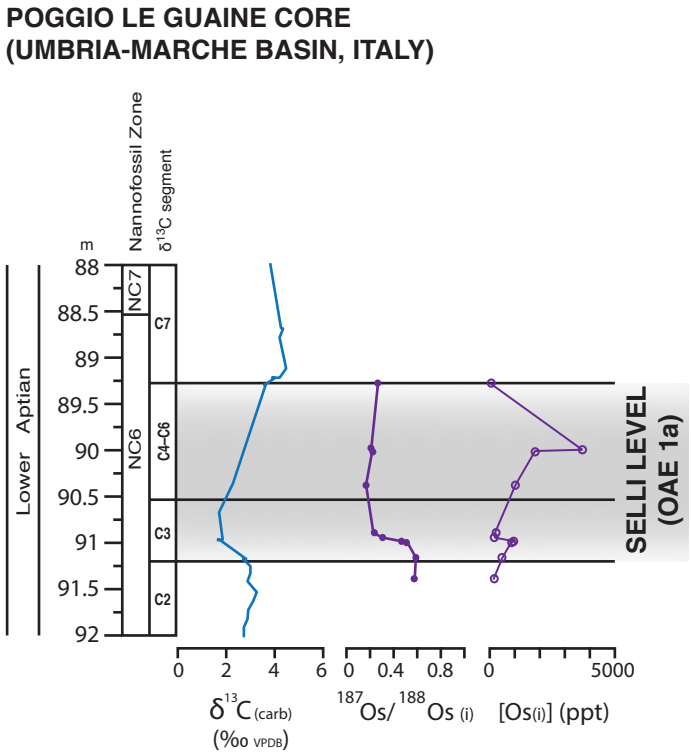
POGGIO LE GUAINE CORE
(UMBRIA-MARCHE BASIN, ITALY)
Lower Aptian
m
88
88.5
89
89.5
90
90.5
91
91.5
92
Nannofossil Zone
NC7
NC6
δ13C segment
C7
C4–C6
C3
C2
SELLI LEVEL
(OAE 1a)
0
2
4
6
δ13C (carb)
(‰ VPDB)
0
0.4
0.8
187Os/188Os (i)
0
5000
[Os(i)] (ppt)

Figure 4

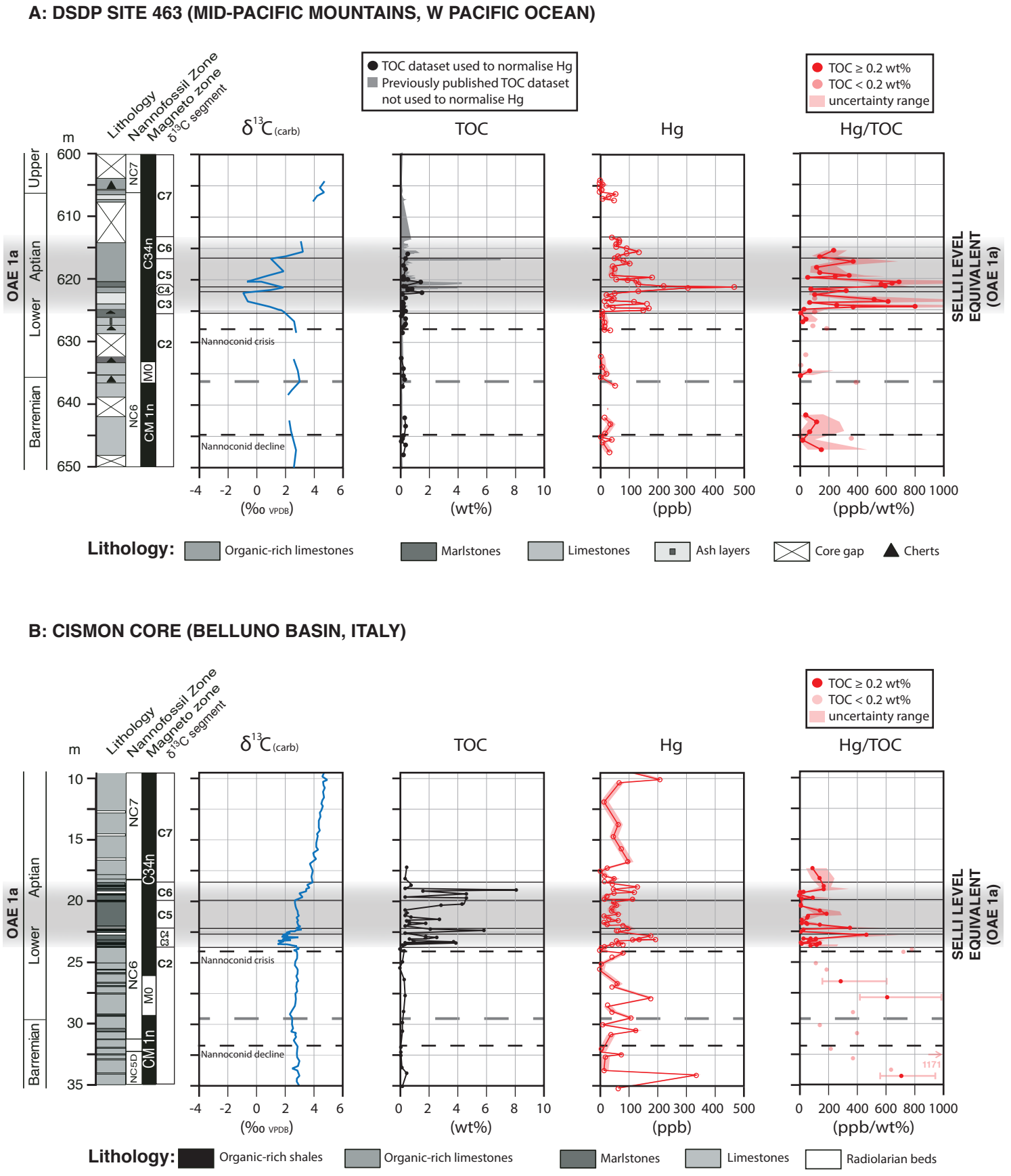
A: DSDP SITE 463 (MID-PACIFIC MOUNTAINS, W PACIFIC OCEAN)
TOC dataset used to normalise Hg
Previously published TOC dataset not used to normalise Hg
TOC ≥ 0.2 wt%
TOC < 0.2 wt%
uncertainty range
Lithology
Nannofossil Zone
Magneto zone
δ13C segment
m
δ13C (carb)
TOC
Hg
Hg/TOC
Upper
Aptian
Lower
Barremian
OAE 1a
NC7
NC6
C7
C34n
C6
C5
C4
C3
C2
M0
CM 1n
Nannoconid crisis
Nannoconid decline
SELLI LEVEL EQUIVALENT (OAE 1a)
(‰ VPDB)
(wt%)
(ppb)
(ppb/wt%)
Lithology:
Organic-rich limestones
Marlstones
Limestones
Ash layers
Core gap
Cherts
B: CISMON CORE (BELLUNO BASIN, ITALY)
TOC ≥ 0.2 wt%
TOC < 0.2 wt%
uncertainty range
Lithology
Nannofossil Zone
Magneto zone
δ13C segment
m
δ13C (carb)
TOC
Hg
Hg/TOC
Aptian
Lower
Barremian
OAE 1a
NC7
NC6
NC5D
C7
C34n
C6
C5
C4
C3
C2
M0
CM 1n
Nannoconid crisis
Nannoconid decline
SELLI LEVEL EQUIVALENT (OAE 1a)
(‰ VPDB)
(wt%)
(ppb)
(ppb/wt%)
Lithology:
Organic-rich shales
Organic-rich limestones
Marlstones
Limestones
Radiolarian beds

Figure 4

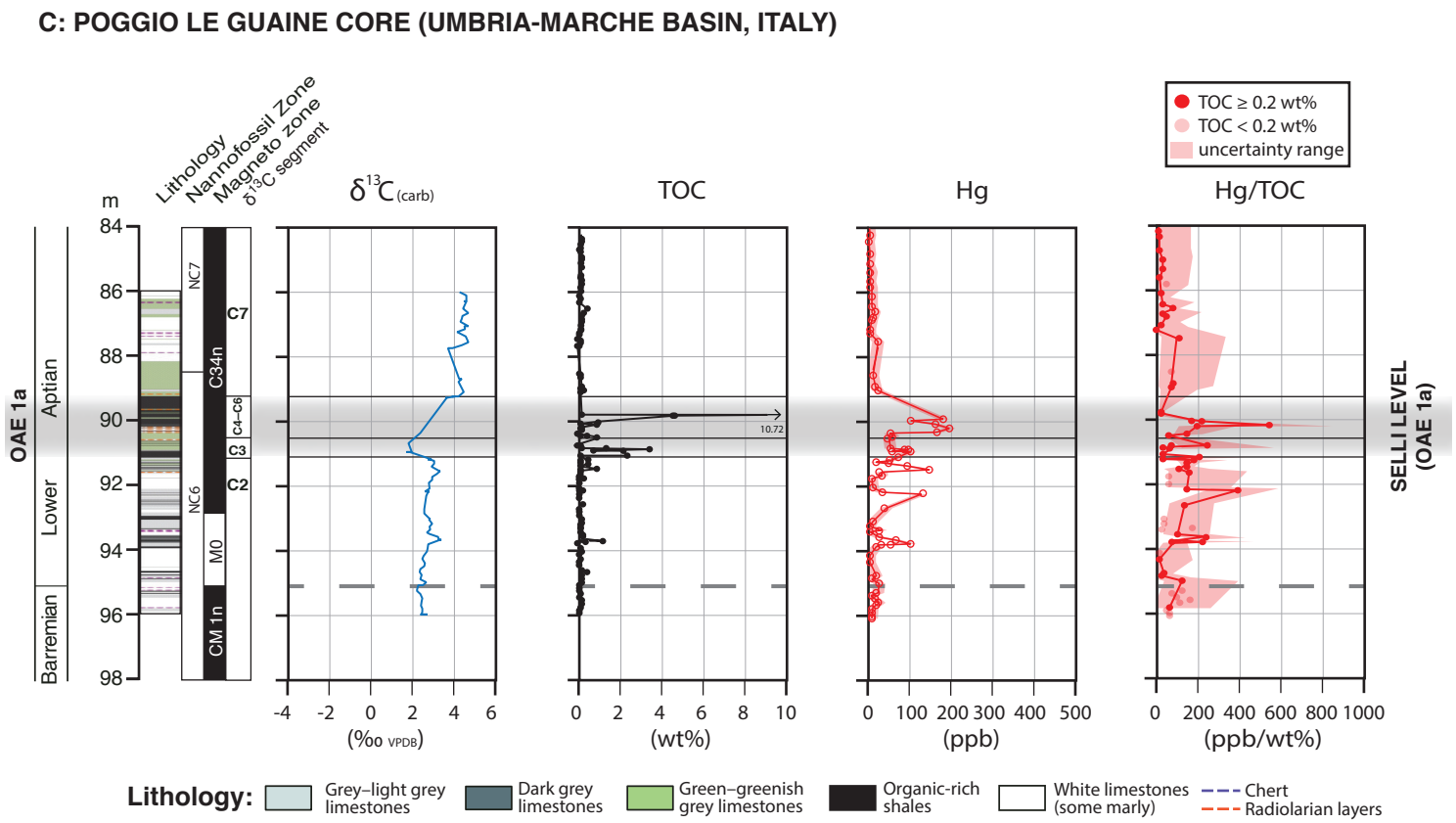
C: POGGIO LE GUAINE CORE (UMBRIA-MARCHE BASIN, ITALY)
Lithology
Nannofossil Zone
Magneto zone
δ13C segment
m
δ13C (carb)
TOC
Hg
Hg/TOC
TOC ≥ 0.2 wt%
TOC < 0.2 wt%
uncertainty range
OAE 1a
Aptian
Lower
Barremian
NC7
NC6
C7
C34n
C4–C6
C3
C2
M0
CM 1n
10.72
SELLI LEVEL (OAE 1a)
(‰ VPDB)
(wt%)
(ppb)
(ppb/wt%)
Lithology:
Grey–light grey limestones
Dark grey limestones
Green–greenish grey limestones
Organic-rich shales
White limestones (some marly)
Chert
Radiolarian layers

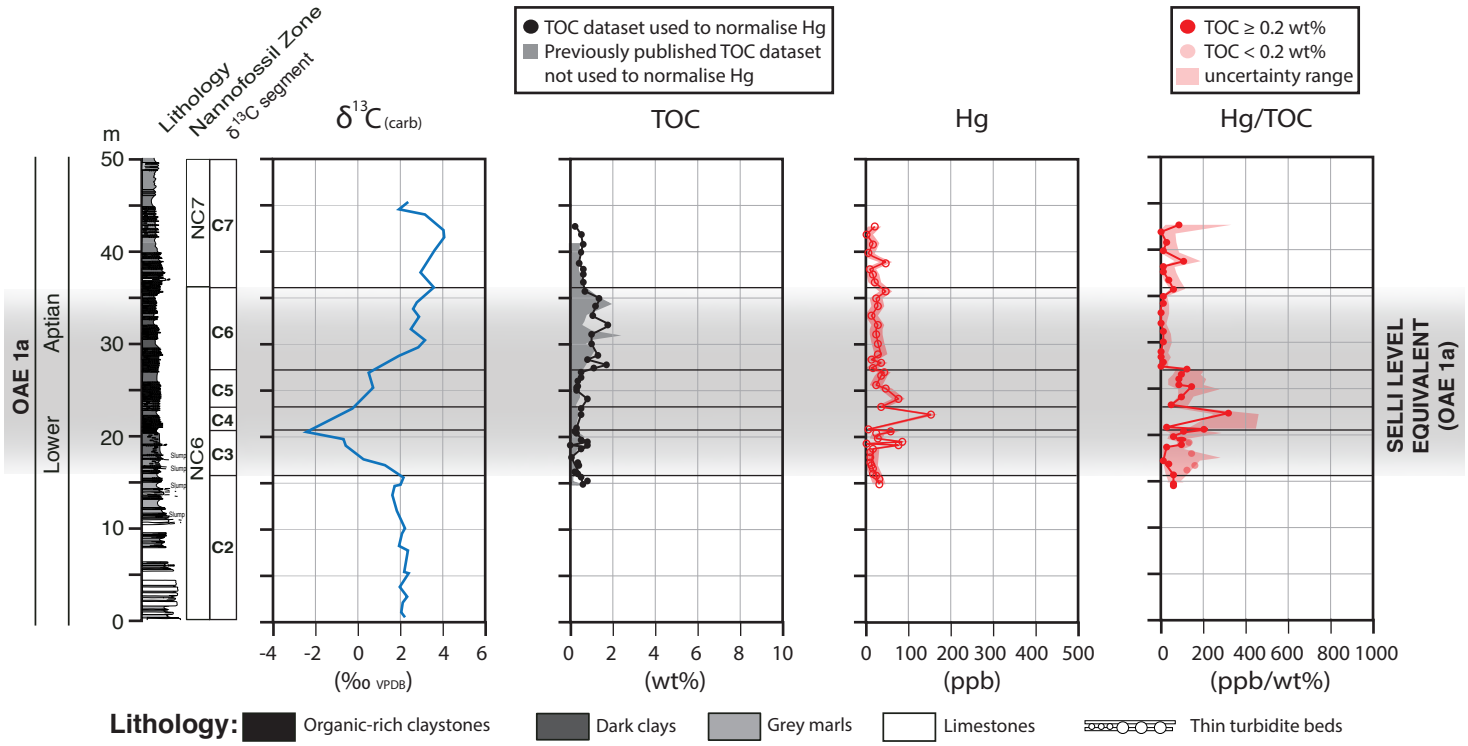
D: NOTRE-DAME-DE-ROSANS (VOCONTIAN BASIN, SE FRANCE)
TOC dataset used to normalise Hg
Previously published TOC dataset not used to normalise Hg
TOC ≥ 0.2 wt%
TOC < 0.2 wt%
uncertainty range
Lithology
Nannofossil Zone
δ13C segment
m
δ13C (carb)
TOC
Hg
Hg/TOC
OAE 1a
Aptian
Lower
NC7
NC6
C7
C6
C5
C4
C3
C2
SELLI LEVEL EQUIVALENT (OAE 1a)
(‰ VPDB)
(wt%)
(ppb)
(ppb/wt%)
Lithology:
Organic-rich claystones
Dark clays
Grey marls
Limestones
Thin turbidite beds

Figure 4

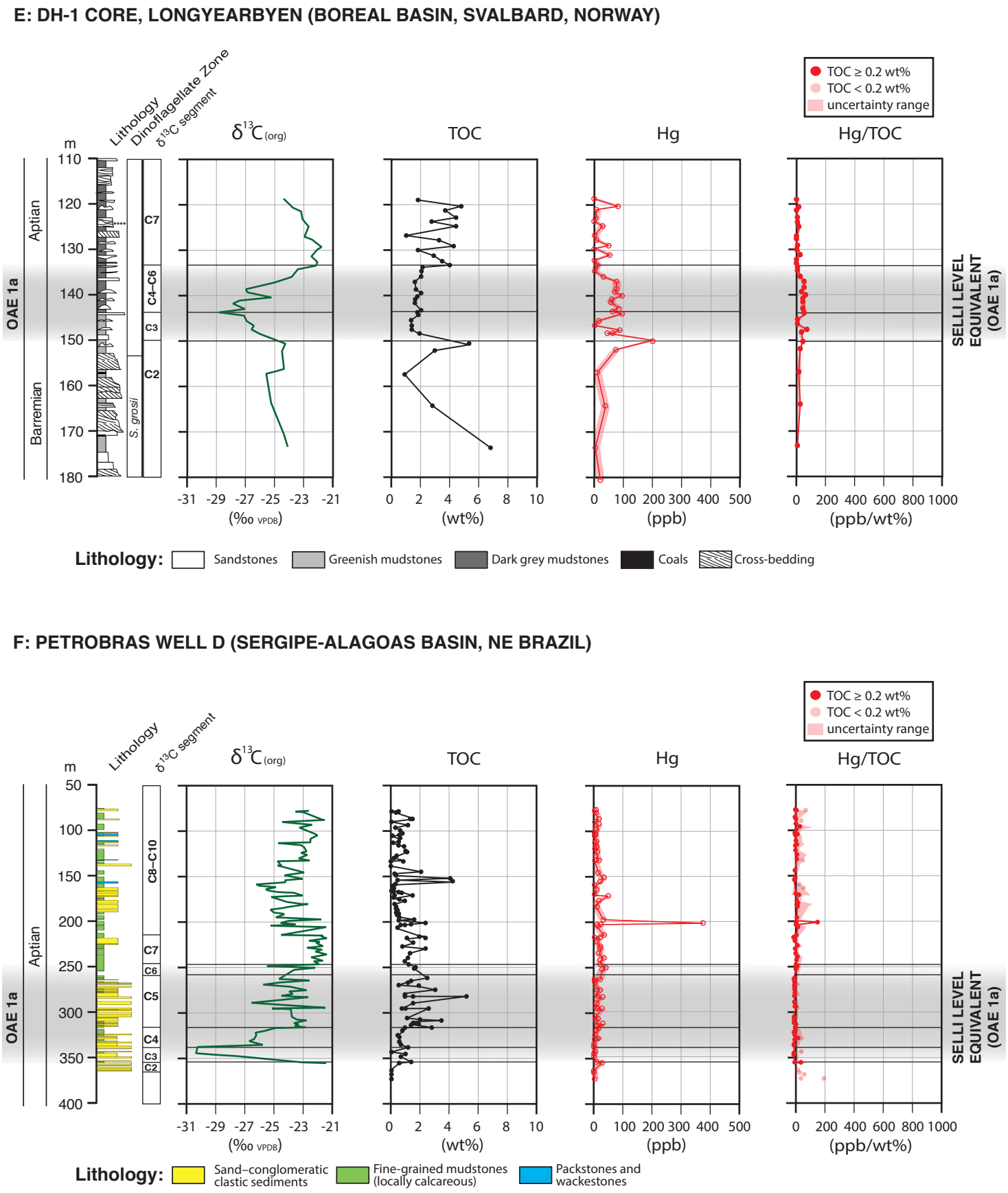
E: DH-1 CORE, LONGYEARBYEN (BOREAL BASIN, SVALBARD, NORWAY)
TOC ≥ 0.2 wt%
TOC < 0.2 wt%
uncertainty range
Lithology
Dinoflagellate Zone
δ13C segment
δ13C(org)
TOC
Hg
Hg/TOC
m
OAE 1a
Aptian
Barremian
S. grosii
C7
C4–C6
C3
C2
SELLI LEVEL EQUIVALENT (OAE 1a)
(‰ VPDB)
(wt%)
(ppb)
(ppb/wt%)
Lithology:
Sandstones
Greenish mudstones
Dark grey mudstones
Coals
Cross-bedding
F: PETROBRAS WELL D (SERGIPE-ALAGOAS BASIN, NE BRAZIL)
C8–C10
C6
C5
Sand–conglomeratic clastic sediments
Fine-grained mudstones (locally calcareous)
Packstones and wackestones

Figure 5

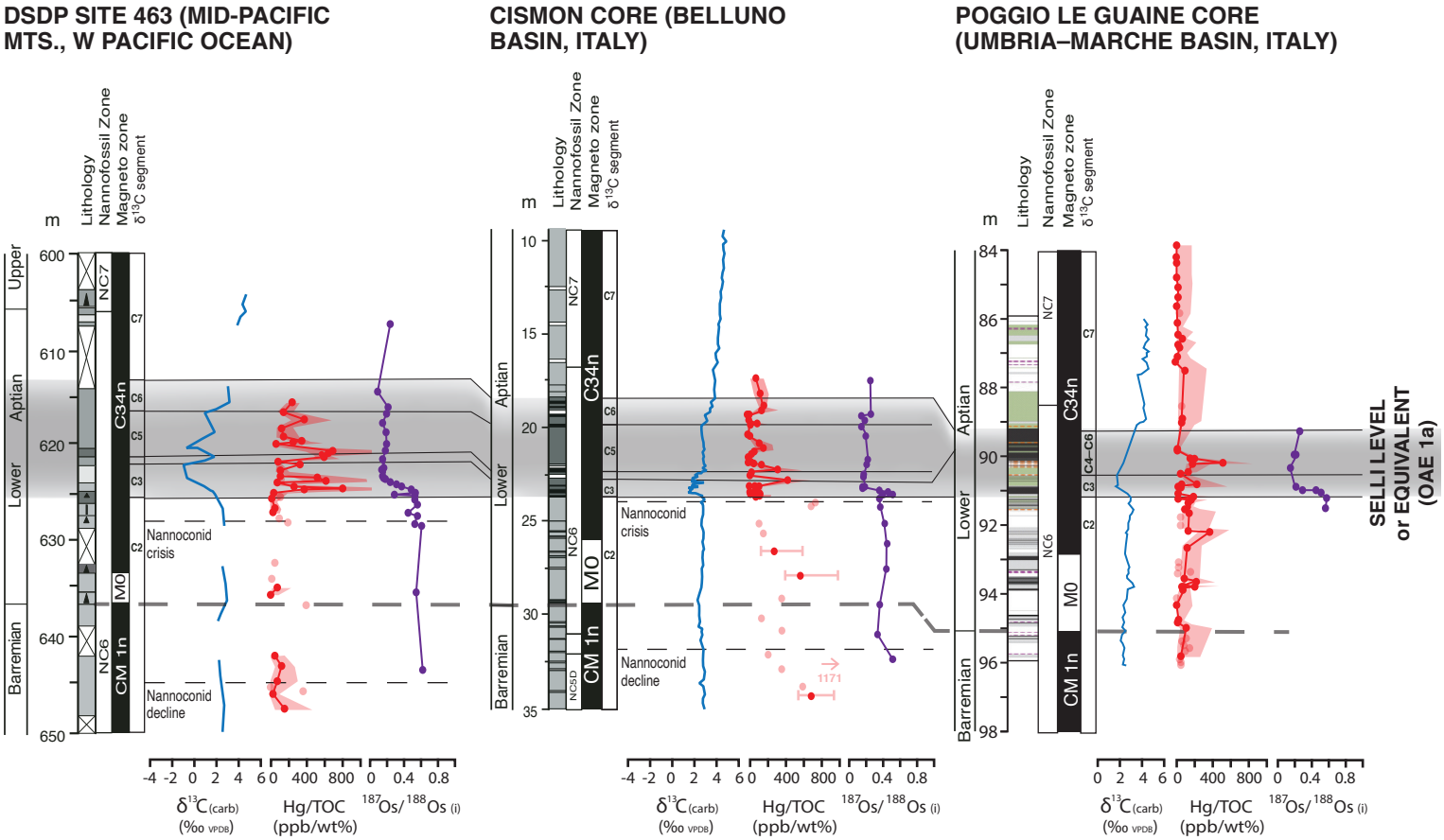
DSDP SITE 463 (MID-PACIFIC MTS., W PACIFIC OCEAN)
CISMON CORE (BELLUNO BASIN, ITALY)
POGGIO LE GUAINE CORE (UMBRIA–MARCHE BASIN, ITALY)
Lithology
Nannofossil Zone
Magneto zone
δ13C segment
m
Upper
Lower
Aptian
Barremian
NC7
NC6
NC5D
C34n
CM 1n
M0
C7
C6
C5
C4–C6
C3
C2
Nannoconid crisis
Nannoconid decline
1171
SELLI LEVEL or EQUIVALENT (OAE 1a)
δ13C(carb) (‰ VPDB)
Hg/TOC (ppb/wt%)
187Os/188Os (i)

Figure 6

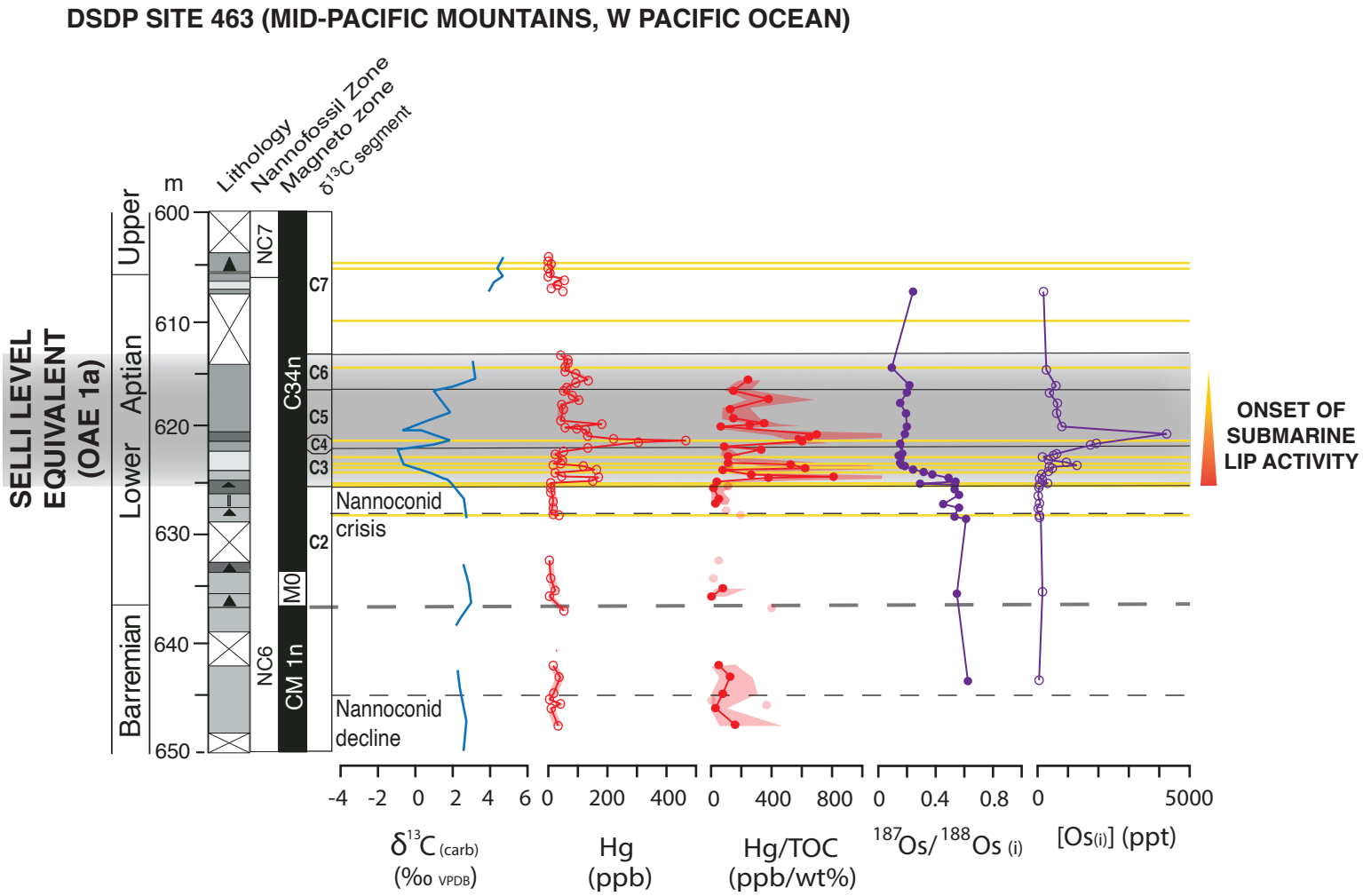
DSDP SITE 463 (MID-PACIFIC MOUNTAINS, W PACIFIC OCEAN)
SELLI LEVEL EQUIVALENT (OAE 1a)
Upper
Lower
Aptian
Barremian
m
Lithology
Nannofossil Zone
Magneto zone
δ13C segment
600
610
620
630
640
650
NC7
NC6
C34n
CM 1n
M0
C7
C6
C5
C4
C3
C2
Nannoconid crisis
Nannoconid decline
ONSET OF SUBMARINE LIP ACTIVITY
-4 -2 0 2 4 6
δ13C (carb) (‰ VPDB)
0 200 400
Hg (ppb)
0 400 800
Hg/TOC (ppb/wt%)
0 0.4 0.8
187Os/188Os (i)
0 5000
[Os(i)] (ppt)